Interfacial polymerization of conductive polymers: generation of polymeric nanostructures in a 2-D space

*Panagiotis Dallas[*1] and Vasilios Georgakilas[2]*

[1] Department of Materials, University of Oxford, Oxford OX1 3PH, UK

[2] Materials Science Department, University of Patras, Patras, Greece

Keywords: interfacial polymerization, conductive polymers, nanofibers, sensors, conductivity

E-mail: panagiotis.dallas@materials.ox.ac.uk; Tel: +44(0)1865273724; Fax: +44(0)1865273789;

Contents

Table of contents/Graphical abstract

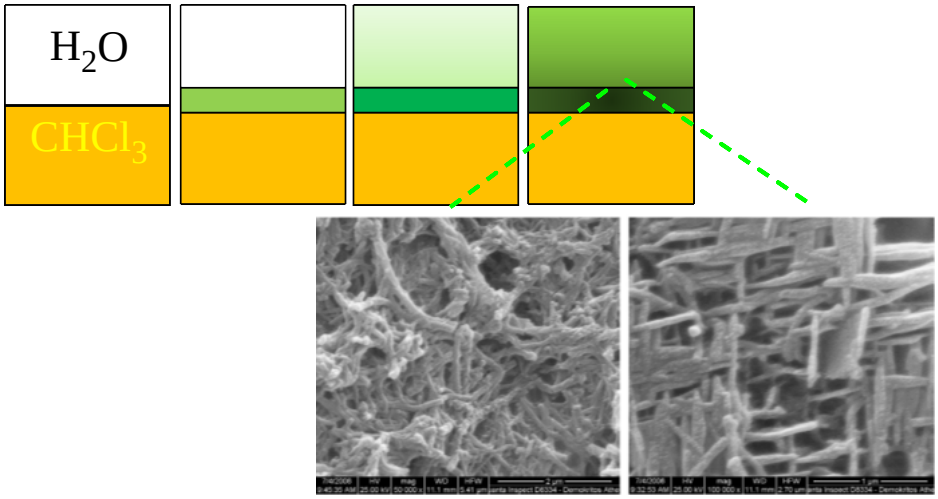

Abstract

In the recent advances in the field of conductive polymers, the fibrillar or needle shaped nanostructures of polyaniline and polypyrrole have attracted significant attention due to the potential advantages of organic conductors that exhibit low-dimensionality, uniform size distribution, high crystallinity and improved physical properties compared to their bulk or spherically shaped counterparts. Carrying the polymerization reaction in a restricted two dimensional space, instead of the three dimensional space of the one phase solution is an efficient method for the synthesis of polymeric nanostructures with narrow

size distribution and small diameter. Ultra-thin nanowires and nanofibers, single crystal nanoneedles, nanocomposites with noble metals or carbon nanotubes and layered materials can be efficiently synthesized with high yield and display superior performance in sensors and energy storage applications. In this critical review we will focus not only on the interfacial polymerization methods that leads to polymeric nanostructures and composites and their properties, but also on the mechanism and the physico-chemical processes that govern the diffusion and reactivity of molecules and nanomaterials at an interface. Recent advances for the synthesis of conductive polymer composites with an interfacial method for energy storage applications and future perspectives are presented.

1. Introduction

Interfaces have a fundamental role in life function and the understanding of their structure, composition and functionality is an important challenge for biomedical engineering, biology, materials science and biomimetics. The most typical example is the living cell membrane. Cell membranes were formed through the assembly of amphiphilic lipopolysaccharides or phospholipid molecules and they enable the selective transport of molecules and ions through them. To that end, biological systems can be viewed as advanced models for the synthesis and construction of numerous biomimetic monolayers, functional materials and devices since they provide an un-paralleled, example of a self-assembled functional structures. In the laboratory, lipid bilayer systems can be readily constructed with the droplet interface approach that can even enable the incorporation of ion channels and pores. [1a] This involves the injection of liposomes in oil films where lipid bilayers spontaneously form. In summary the study of the biological two phase

systems presents an important challenge in the field of biomimetics. [1-2] Furthermore, and this is a key aspect in polymer chemistry, at the two dimensional (2-D) liquid-liquid interface boundary, completely different properties compared to the separate aqueous and organic phases can be found. In fact, the interface can be considered as a separate and new entity, with a complex structure and a thickness of less than 1 nm where electron and mass transfer can take place. [3]

The chemical and physical processes that occur in the interface between an organic and an aqueous solution can be substantially different than those occurring in a homogenous, single-phase, reaction mixture. [4] The interface can be considered as an imaginable membrane through which selective flow and transitions can take place. Consequently, the reactions at the boundary between two immiscible liquids play an important role in fields such as analytical chemistry, organic chemistry and biochemistry. [5] Reactions at the liquid/liquid (denoted as L/L) interface have been reported in various systems. Typical processes include photo-induced electron transfer [6], organic synthesis [7], charge transfer even between photosensitizers and quenchers [8], and phase-transfer catalysis [9] and ion-pair extraction [10]. Noteworthy is the phase-transfer catalysis, (PTC) which facilitates chemical reactions between reactants in two immiscible phases and is one of the most important techniques in organic synthesis. [11] By the virtue of supramolecular interactions the liquid–liquid interfaces [12a] offer an important scaffold for the organization of nanomaterials, typically inorganic nanoparticles and viruses [12b] by exploiting the different hydrophobic or hydrophilic character of the constituent members of the reaction

In polymer science the interfacial polymerization method is already known to produce relatively high molecular weight products for a series of conventional polymeric materials like polyamides, polyesters and polyurethanes which are synthesized through radical mediated addition or condensation polymerization [13-14]. Compared to these polymers, the unique characteristic of conductive polymers is their charged macromolecular chains, their oxidative polymerization mechanism and the constant need for the synthesis of ultra-small nano-structures and fibrillar, elongated morphologies that can conduct electricity and also exhibit a rapid and reversible response as sensors. As such, the interfacial polymerization of conductive polymers creates a common ground of nanoscience, materials science, polymer chemistry and physics, and organic chemistry.

The characteristics of the interfacial reactions have extensively been studied from the viewpoint of physical chemistry and electrochemistry. The electron, ion and mass transfer as well as the polarity and thickness of the interface between these two immiscible liquids have been the focus of intense research. In these two-phase systems diffusion phenomena between the immiscible phases, a slow reaction rate and a restricted reaction space govern the formation of various products. The technique has been studied in the context of numerous applications in membrane and polymer science. Examples include the bulk polymer synthesis of polycarbonates [15, 16] and other polymeric materials [17], a range of different applications and families of materials such as micro/nano-encapsulation [18–19], thin film composite and nanocomposite membranes [20–25], polyamides reinforced with carbon nanotubes for reverse osmosis [25b] and other polymer nanocomposites formation [26-27]. It has also attracted attention in the

context of surface modification of fibers [28, 29], micro-units [30, 31] and self-healing materials. [32]

The discovery of conductive polymers has opened up many new possibilities for electronic devices and sensors due to the combination of a range of controllable, exciting, optical, electrochemical, and conducting properties. These polymers demonstrate instant and easily detectable electrical and optical changes when they are chemically treated with oxidizing or reducing agents. After chemical treatment with redox active agents, conductive polymers immediately change from an insulating to an electrically conducting state and vice versa [33-34]. These transitions between different states can be particularly useful in applications such as optical sensors [35] chemical sensors [36] and biosensors. [37] The most widely studied conductive polymers include polyaniline (PANI), polypyrrole (PPY), and poly-(3,4-ethylenedioxythiophene) (PEDOT). They have been synthesized through oxidative interfacial polymerization, utilized as matrices for the incorporation of numerous nanostructures and have found applications in many and diverse areas. In all these applications the uniformity of the polymers morphology and the specific morphological characteristics are playing a vital role making the interfacial polymerization a versatile tool for the synthesis of conductive polymers fibers, films and composites.

We will firstly present an overview of the characteristics of the L/L interface. As a second step we will critically discuss how it influences the formation of elongated nanostructures and the advantages it represents in terms of conductivity, crystallinity and sensor applications. Our discussions is focusing on the oxidative polymerization of

conductive polymers. We will close our review with presenting and critically addressing the recent progress in the field of energy storage applications.

2. The boundary between two immiscible liquids

2.1. Overview and theoretical background

In the field of materials science and nanotechnology, the liquid-liquid medium has been employed for the synthesis of polymeric nanoparticles, films of metallic nanoparticles in the interface including highly crystalline and photoluminescent metal chalcogenides, metal oxides, and noble metal nanoparticles. [38a] The process involves the assembly of the inorganic nanoparticles at an oil–water interface, localized in a place where the interfacial tension is high. In this system, the self-organization is a highly dynamic process, the particles move rapidly and try to self-assemble and equilibrate and this enables errors to be corrected immediately. Similar processes have been known and studied for over 100 years and have been denoted as “Pickering emulsions” in which large particles, for example silicon oxide, (diameter, d>1 mm) stabilize emulsions efficiently by adsorption to a liquid–liquid interface. [38b] The high interfacial energy between oil and water can be decreased by the assembly of the NPs at the interface; in fact it is interesting that during the interfacial polymerization, polymer nanoparticles are formed at the interface thus further decreasing the interfacial tension between these two liquids. This decrease in surface energy favors the formation of a monolayer of NPs located at the interface even if this decrease is counterbalanced by the kinetic energy of the NPs in solution due to Brownian motion. [39]

Since the L/L interface can be considered to be a flat surface with a height of maximum 1 nm, the polarity is expected to be different compared to the two constituent, separate entities members. [4] Various publications has demonstrated that indeed the interface is a thin layer having a polarity that lies exactly in the middle of the polarities of the two liquids [40-41]. However, the interface is not entirely flat, neither sharp nor continuous and fluctuations occur either lateral or normal to the interface. A study by Tauer et al based on light microscopy observations of organic liquids and water demonstrated that solutes are moving towards both sides of the two solutions, the aqueous and the organic phase. The formation of droplets that are not uniformly distributed in the interface and migrate to both phases has been observed with light microscope. This means that water aggregation takes place at the organic phase and hydrophobic molecules aggregation in the aqueous phase. [42]

Bessho et al. applied time-resolved total-internal-reflection (TIR) fluorescence spectroscopy to the study of microenvironments around 8-anilino-1-naphthalenesulfonate (ANS) at a water/heptane interface, and they suggested that the interfacial polarity was intermediate between those of heptane and water. [43] According to Ishizaka et al [44a] and Wang et al [44b], the interfacial polarity ($P_{A/B}$) in the boundary of the two immiscible liquids (*A* and *B*) is equal to the average of the polarity of the two bulk phases (P_A and P_B). The applicability of this assumption was generalized, checked and established for a series of two-phase systems, like water/*n*-heptane, water/*n*-decane, and water/cyclohexane interfaces.

If the molecules, the products of the reaction, are charged they will remain in this state in both the interface and the aqueous phase while they will migrate as neutral

species in the organic phase. This is the case of polyelectrolyte polymers like polyaniline or polypyrrole. An interesting aspect is that their oxidation states and the level of protonation can lead to three different derivatives: water-dispersible polymers or charged oligomers in the aqueous phase, non-charged neutral oligomers in the organic phase and an insoluble thin film at the interface. Thus by proceeding the reaction in a two-phase system an one-step separation of all the different states can take place.

2.2. Electron and mass transfer in the boundaries of two immiscible liquids

When an ion is transferred at the interface between water and an organic liquid, a current is flowing across the interface and the difference in the potential between the two solutions is proportional to the number of the charged electrons that are transferred across the barrier. The redox reaction take place at the interface and the oxidized and reduced species may return to the preferred phase (Figure 1). [4] The ion transfer and the electron transfer can be considered as electrochemical processes. Due to these gradients, energy conversion reactions occur at biological membranes. [45]

In laboratory, various systems have been used in the previous decades as model systems for the study of interface interactions. For example, in 1979 Samec et al [46] reported an electron transfer between ferrocene that is dissolved in nitrobenzene (nb) and $Fe(CN)_6^{3-}$ dissolved in water. This electron transfer can be presented in the following equation:

$$Fc(nb) + Fe(CN)_6^{3-}(water) \leftrightarrow Fc^{+}(nb) + Fe(CN)_6^{4-}(water)$$

Figure 1.

The redox reactions at the interface between immiscible liquids can be classified in two different categories. The first category includes spontaneous processes which can be chemical reactions that occur in the absence of external electromagnetic field. This type of redox transformation has been investigated in bioenergetics, model membrane systems, nanocrystalline thin films [47a] at oil/water interfaces. Redox reactions of the second type [47b] occur at the interface when external electrical fields are applied to the interface, for example with cyclic voltammetry in an electrochemical cell. Under an applied voltage interfacial charge transfer reactions take place at controlled interfacial potentials. Such electrochemical interfacial reactions are usually multi-stage processes that proceed through the following steps, which are similar to the paths followed in interfacial catalysis [47b-c]:

(i) The reactants diffuse to the interface;

(ii) Adsorption onto the interface;

(iii) Electrochemical reaction: external electric field is applied

(iv) The products are moving away from the interface;

(v) The products diffuse to the two liquid phases or thin film formation at the interface.

We have already mentioned the cell membrane system as a fundamental interfacial model. An important example of electron transfer coming from the biological world concerns the photosynthetic pigment, the chlorophyll. The Chlorophyll class of biological pigments has a role of utmost importance since these are the molecules that

mediate the primary act of photosynthesis in higher plants. However, chlorophyll molecules can also catalyze electron transfer reactions at oil/water interfaces and on bilayer lipid membranes [48]. The redox properties of chlorophyll *a* and *b*, the two main types of chlorophylls, were studied in an early work by Rabinowitch and Weiss who observed the following homogeneous redox reaction of chlorophyll (Chl) with ferric chloride:

$$Chl + Fe^{3+} \rightarrow oChl^{+} + Fe^{2+}$$

oChl: oxychlorophyll, a yellow oxidized form.

If ferric salts are added to chlorophyll dissolved in methanol (CH_3OH), the solution changes color from green to yellow, and spectroscopic analysis of the products demonstrated a significant suppression and decrease of absorbance intensity of the chlorophyll adsorption spectrum. In a water/oil system, chlorophyll molecules that are adsorbed at the interface catalyze the electron transport between donors and acceptors located in the two phases. The chemical structure of the chlorophyll *a* molecule merits for its high catalytic activity at the oil/water interface since it is an amphiphilic molecule consisting of a hydrophilic head formed by four pyrrole rings with polar carbonyl groups located around a magnesium ion and a long hydrophobic, aliphatic chain, or "tail" as it is commonly named.

2.3. Mass diffusion in the interface (Molecular recognition at an interface)

Mass transfer from the bottom to the upper phase mediated through the interface can also take place. This effect has been observed in polymerization reactions that will be later discussed. Typical example is the molecular recognition in biological systems that proceed at microscopic interfaces such as cell and protein surfaces in aqueous media.

Therefore hydrogen bonding interactions at a liquid/liquid interface have received interest as a model of molecular recognition in biological systems. For example, riboflavin a surface active dye can form hydrogen bonding complexes in an aqueous/oil interface with diamino-s-triazine. The latter acts as a flavin receptor via triple hydrogen bonding [49] and alkali metals have been observed to complexate with crown ethers at a water/heptane interface. Li^+, K^+ and Li^+ are examples of ions that formed complexes with a crown ether in a study by Nochi et al. [50]

Srivastava and coworkers programmed the assembly of nanoparticles at an interface driven by interaction among DNA macromolecules. [50b] The ionic strength of the solution controlled by the addition of NaCl salt dictated the assembly of the nanoparticles and the rheological properties of the membrane that was formed on the interface. The system is dominated by a competition between a charge induced repulsion and a DNA induced attraction and in situ Small Angle X Ray Scattering studies of the interface revealed the phase transitions. Furthermore, Sanyal and coworkers demonstrated an arrangement of gold nanoparticles at an interface similar to Au-55 nanoparticles with each cluster consisting of 13 nanoparticles. [50c]

2.4. Surface tension at the liquid-liquid interface

Surface forces dictate the properties of the surface in any class of materials. In effect, they are the summary of all forces acting between the particles, as also the particles and the medium that surrounds them. This collective interaction and forces gives rise to the surface tension. The microscopic origin of the surface tension lies on the unfavorable state of matter at the interfaces and the intermolecular interactions. [51]

Atoms or molecules at the surface are surrounded by other atoms or molecules with different characteristics and behavior, in contrast with the interior molecules that are surrounded by similar moieties thus minimizing the energy of the system. [51b] This model can be expanded in the case of a liquid-liquid interface. [52] Fisk and Widom mean field theory [52b-52c] tried to clarify the features of the liquid-liquid and liquid-vapor interface and was predicting that the surface tension would depend upon the density profile of the two liquids. Their work expanded previous theories and presumed homogeneity of the interface to estimate the surface tension. [53] However the overall picture appears to be more complicated since thermal and density fluctuations should be considered, portraying a rough interface. [54] Buff, Lovett and Stillinger analyzed how transverse fluctuations that cause macroscopic displacements on the interface, while Aarts et al [55] studied the fluid-fluid interface in a polymer dispersions with laser scanning confocal microscopy [56]. Fluorescently labeled poly(methylmethacrylate) were monitored with laser scanning confocal fluorescence microscopy Their studies directly observed thermally induced capillary waves at the interface proving the roughness of the interface.

A pioneering paper by Fowkes et al suggested that the surface tension should be considered as a sum of independent terms each representing a particular intermolecular force [57a], or the excess of energy due to the unfavorable configurations at an interface [57b]. For instance the surface tension of water (w) whose main intermolecular forces are hydrogen bonding (h) and dispersion forces (d) can be described by the following equation: $\gamma_w=\gamma_w^h + \gamma_w^d$. On the other hand a hydrocarbon (γ_c) will have a surface tension that is dependent only on the dispersion forces. So in a water-hydrocarbon interface only

the dispersion forces will be applicable and the surface tension of a water-hydrocarbon interface can be described by the Good-Girifalco equation: $\gamma_{cw}=\gamma_c + \gamma_w -2(\gamma_c\gamma_w^d)^{1/2}$. [57c]

We will now present the applications of the theoretical approaches on the interface structure in the formation of polymeric nanostructures. An interesting and smart method that uses the interfacial properties of immiscible liquids has been presented in the work by D Arcy et al. The authors demonstrated a solution-based method for growing transparent thin films of nanofibers of polyaniline, polythiophene, and poly (3-hexylthiophene) on various substrates. The method is based on emulsification of two immiscible liquids and pre-synthesized polymer nanofibers. An interfacial surface tension gradient, viscous flow of the solution and efficient film spreading lead to a growth of a transparent film of a series of conductive polymers in short time. [58] In fact, surface tension gradients have previously been used to form inorganic nanoparticles films. [59] The films presented by the Kaner group are of conductive polymers and possess remarkable nanoscale order. This order is reflected in the formation of a series of nanofibers monolayers and the advantage of this smart method is the control of the precise morphological homogeneity, its simplicity and potential scalability for bigger films. The results indicated that the interfacial surface tension controls the nanoscale morphology while the film growth is driven by the tendency of minimization of the total interfacial surface free energy of the system. [60] A greater interfacial surface tension pulls on the nanofibers with a stronger force and allows a film to climb up the substrate against gravity, leading to greater spreading heights. As a conclusion the work revealed that the formation of Nanofiber films was dependent to the immiscible liquids that were chosen and to how high was the surface tension at their interface. Typical values of the

interfacial tension for the pairs that were studied are: H_2O/CCl_4 - 45 dyn⁄cm, $H_2O/CHCl_3$ 32.8 dyn⁄cm, and the lowest value corresponds to the H_2O/CH_2Cl_2 system- 28.3 dyn⁄cm. As a final step, P3HT field effect transistors were also constructed and displayed a mobility of 2.7×10^{-3} cm^2/Vs. [58] In the following chapters we will provide more insights on the polymerization mechanism of aniline and pyrrole in an interface and the formation and evolution of nanostructures.

3. Interfacial polymerization of aniline and pyrrole

3.1. Aniline

3.1.1. Formation mechanism of nanofibers at the interface

Polyaniline is among the most studied conductive polymers, mainly due to the combination of high conductivity, various different oxidations and protonation states each one exhibiting different color and electronic properties, light weight, easy preparation and low cost. [61] Its ability to form ultra-small nanostructures, including nanowires, nanoneedles and nanofibers has been proven particularly useful in the application of the polymer in sensors applications since their extremely high specific area enables the fast detection of small molecules that can cause immediate changes in the oxidation states and as it is expected to the conductivity values and the optical absorption spectrum, the latter can exhibit from one to three absorbance bands depending on the polymer form.

Taking into account the previously mentioned studies we can propose a mechanism that will model the mass diffusion and mass transfer in a two phase reaction (Figure 2a). We can assume that in a chloroform-water system aniline is oriented with the polar group heading towards water where the oxidation takes place while the non-polar

group is headed towards the organic phase. When the first oligomers are formed the restricted 2-D space of the interface suppresses the secondary growth of the polymer and elongated anisotropic structures are formed.

Figure 2.

Isolation of oligomers and polymers in the various stages during the polymerization of aniline demonstrated that the fibrilar morphology is an intrinsic characteristic of the polymer nature and the irregular and globular shapes are formed in the so-called secondary growth of the macromolecules. [62] Consequently if the first nucleation step and the secondary growth step are separated the fraction of nanofibers/nanoneedles and nanospheres can be easily controlled. Therefore, if the secondary growth is further suppressed, the yield of nanofibers in the final product could be substantially increased and the exclusive isolation of elongated and anisotropic structures is feasible. The interfacial polymerization represents an effective method for exactly this reason: it suppress the secondary growth. Since the monomer (aniline) and the initiator ammonium peroxydisulfate are separated by the boundary between the aqueous and the organic phase, polymerization occurs only at this interface, in the space where all the components needed for polymerization come together [62]. Polyaniline then grows and self-assembles in the desired structures, e.g. Nanoneedles, nanofibers or nanorods. [63-65]

Since these newly formed nanofibers are in the doped emeraldine salt form, they are hydrophilic and can rapidly move away from the interface and diffuse into the water phase (Figure 2b). In this way, as the nanofibers form they are continuously withdrawn from the reaction front, thus avoiding secondary growth and allowing new nanofibers to

grow at this interface. This effect explains why nanofibers [65] or nanoneedles (Figure 3) [66] are obtained no matter which solvent is used as the organic phase in interfacial polymerization.

Compared to the conventional aqueous-phase synthesis, in an interfacial polymerization are fewer nucleation sites to enable the initiation and propagation of the polymer reaction. [63a] In the single-phase synthesis, the initiator (oxidizing agent and/or acid) molecules are mixed in a three-dimensional space with the monomer molecules in bulk solution under constant stirring. Each oxidized monomer then can potentially create a nucleation center for a polymer chain growth. However, in interfacial polymerization, the interaction between initiator molecules and monomers are essentially limited to the restricted two-dimensional space the aqueous/organic interface, without any stirring and the nucleation and chain propagation takes place there.

Another quite similar path with this reaction involves polymerization of aniline in the monolayers of lipid membranes. As it is well known the aniline monomer is protonated by strong inorganic and organic acids to the anilinium cation during the first stages of the polymerization. This aromatic cation can be strongly adsorbed at the charged monolayers of the phospholipids L-α-dimyristoylphosphatidic acid (DMPA) and hexadecanesulfonic acid (HDSA) at the air–water interface, and may undergo chemical polymerization with the organic surfactants acting as templates. [68]

3.1.2. Other morphologies that can be generated at an interface

Simply by altering the concentration of the surfactant added, for example cetyl trimethylammonium bromide (CTAB), during the oxidative polymerization various

morphologies from needle shaped (CTAB concentration 0 mol/l) to rice like (0.02 mol/l) and hollow microspheres (0.04 mol/l) and wires (0.06 mol/l) were observed. [70a] This needs to be correlated with the critical micelle concentration of CTAB in water, which has been estimated to be 0.92 mM. [70b] In the work by Li et al the surfactant was dissolved in the aqueous phase and the monomer in chloroform. In the interface and colloids science it is well known that amphiphilic surfactants will arrange themselves in an aqueous solution in a specific and preferable way. The polar groups are arranged towards the aqueous phase while the aliphatic chains head towards themselves avoiding the water molecules and create spherical templates that govern the growth of the polymer chains. These spherical templates suppress the tendency of the polymer to grow in one dimension and more isotropic or even hollow structures are formed. As we have already discussed, in interfacial polymerization without the addition of a surfactant, Huang and Kaner proposed that this polymerization is an effective method to suppress secondary growth of polyaniline by removing the nanofibers from the reactive interface. In a traditional homogeneous reaction system in the presence of a surfactant, micelles formed by the surfactant ions were regarded as templates in the formation of the nanostructures. On the other hand, during the interfacial polymerization process, special micelles might be formed in the interface between water and the organic solution. These micellar templates are different from the traditional micelles formed in a homogeneous reaction system in the presence of a common surfactant.

The spherical micelles that are formed in the reaction might be regarded as “templates” in forming the three dimensional hollow microspheres through a self-assembly process in the oil–water interface. According to the work Li et al an increasing

CTAB concentration causes the morphology of micelles to change from spherical to linear and this leads to 1-D nanowire with network structure. [70a] Expanding the gallery of available nanostructures of polyaniline through interfacial polymerization, cyclic nanostructural polyaniline has been synthesized by means of a slightly modified method where polyacrylic acid was employed. [69] Ding et al reported the fabrication of DBSA-doped polyaniline nanorods by interfacial polymerization, however according to the UV-Visible spectrum the polyaniline seems to be in the non-doped and insulating state, meaning that the doping level is decreased due to the presence of DBSA and xylene. [72]

In summary, depending on the organic solvent that is used the interfacial reaction may proceed in a different way depending on it polarity, surface tension, solubility of the products and gravitational factors, for example if the organic solvent is lighter than water, i.e. toluene or xylene, then the water phase is the lower phase and the polyelectrolyte chain of polyaniline will be forced to migrate there.

Figure 3.

3.2. Interfacial polymerization of pyrrole

In contrast with polyaniline that is a slightly hydrophilic polymer and can be solubilized in water upon high dilution, polypyrrole is a completely insoluble polymer in any solvent either organic or water. With respect to the above, the interfacial polymerization seems an excellent candidate for the synthesis of a thin film in the boundary of the two phases. This thin film can be easily extracted and purified. The poor solubility of polypyrrole in any solvent has been assigned to an extensive cross-linking

between the polymer chains. [73] Oligomers however, tend to be easily dispersible as we will later discuss.

The polymerization of pyrrole involves oxidation of the monomer with metal cations, for example ferric ions from iron nitrate salts dissolved in aqueous solutions. Usually the polymerization of pyrrole takes place in water and the reaction leads almost immediately to the insoluble black powder polypyrrole, a charged polycation with nitrates as counterbalancing anions. The redox potential of typical ions like Fe^{3+} (E=0.77 Volt) and Ag^{+} (E=0.80 Volt) is enabling them to serve as initiators of the reaction and the polymerization proceeds almost exclusively through attack in the a-position of the five-membered pyrrole ring (Figure 4).

What will happen if the initiator ions and the monomer are added in separate phases, the first in the aqueous and the second in the organic phase, thus exploiting the previously mentioned characteristics of the interfacial boundary? Again, the polymerization will proceed through oxidation of the pyrrole monomer, this time in the interface which represents a restricted two-dimensional space. As the polymerization proceeds a minor percentage of charged oligomers migrate to the aqueous upper phase, but when the molecular weight becomes sufficiently high, an insoluble thin film starts forming at the interface and can be easily cast. At that point there is no ion flow between the two phases and immediately the polymerization is terminated.

A three-dimensional network consisting of branched polypyrrole fibers has been synthesized by interfacial polymerization method in the presence of sulfonated β -cyclodextrin (Sβ-CD) that acted as the doping agent. The authors investigated the effect of synthesis conditions such as the concentration of the Sβ-CD in the polymerization

media, the type of oxidant that was used to initiate the reaction and the temperature on the electrical properties of polypyrrole-Sβ -CD. [74] A similar use of cyclodextrin for the interfacial polymerization of aniline has already been reported. [75] In this synthesis chiral polyaniline nanobundles were prepared by interfacial polymerization using immiscible organic/aqueous biphasic systems. The chiral nanostructures arise from the intertwining of polyaniline chains over interconnected units of cyclodextrin sulfate. Interestingly, the formation of chiral polyaniline nanobundles was witnessed only in the aqueous phase, irrespective of the organic solvent used in the interfacial polymerization. [75]

3.3. Conductive polymer nanocomposites

3.3.1. Noble metal nanocomposites

The reaction mechanism for the polymerization of pyrrole is exactly the same when instead of iron nitrate; silver cations are used as initiators. The silver cations are reduced and simultaneously are oxidizing the pyrrole monomers thus initiating the chain propagation. In this case, the polymerization is simultaneously creating zero-valence silver nanoparticles that are immediately trapped inside the growing polymer chains. This results to the formation of small silver nanoparticles finely dispersed inside a conductive polymer matrix with a narrow size distribution. [76] The exact percentage of the silver in the polymer composite can be estimated through thermogravimetric analysis (TGA) which provides a good estimation of the percentages of silver and polymer. As an example, for a molar ratio of the monomer to the initiator 0.5 ml (7 mmol) pyrrole /180 mg $AgNO_3$ a 60 % wt of the composite was silver nanoparticles.

Figure 4.

During the polymerization, the Ag^+ cations are reduced to metallic silver, and the formation of regular nanocomposite materials was established by transmission electron microscopy (Figure 5). The silver nanoparticles had a diameter between 5-10 nm and the method can be expanded to other noble metals that can be readily reduced, like gold, platinum or rhodium. Thermogravimetric analysis and differential thermal analysis were carried out to study the thermal stability of the resulting composites. [74] In a similar manner polyaniline-silver nanocomposites were prepared by employing interfacial polymerization using ammonium persulfate as an oxidizing agent.

Gold nanoparticles with various sizes and shapes have been synthesized by exploiting the suitable redox potentials of poly (o-methoxy aniline) and gold chloride. Spherically shaped and truncated pentagonal/hexagonal shaped nanoparticles where synthesized and were dispersed inside the polymer matrix. [77]

3.3.2. Carbon nanotubes and graphene nanocomposites

The incorporation of silica [78] carbon nanotubes or most recently graphene, [79] in polymer matrices, especially conductive polymers, is highly anticipated especially since carbon nanotubes have long been recognized as the stiffest and strongest man-made material known to date and graphene is proposed to revolutionize materials science. Furthermore, their high electrical conductivity has made carbon nanotubes strong candidates for applications in the area of electrical appliances and communication related applications. [80] Interfacial polymerization has expanded the available methods for the synthesis of carbon nanotubes nanocomposites especially towards the efficient grafting of

the nanotubes with a polymer layer. Typically, organophilic carbon nanotubes that are added in the bottom organic phase can be entrapped by the significantly more hydrophilic, low molecular weight pyrrole oligomers and being transferred in the aqueous phase until the molecular weight becomes very high. In the latter case the composite is trapped in the interface as a thin film. [81-82] In the work by Georgakilas et al [81a] and Han et al [81b] organophilic, functionalized with oleic acid, carbon nanotubes and pyrrole monomers were dispersed in the bottom chloroform phase and iron nitrate in the upper aqueous phase. The conventional polymerization of pyrrole takes place in an aqueous phase where the monomer has a solubility 7.5 % wt. and readily forms the polypyrrole black powder after the addition of the oxidizing agent. [82] When the monomer and the oxidant are added in two different phases the reaction proceeds with an interesting way: ferric ions diffuse in the interface where they react with pyrrole monomers. The polarity of the interface lies between the two solvents so the oxidation of the pyrrole and diffusion is feasible as has been previously discussed. Notably, the reaction continues to proceed in the chloroform phase where there is an excess of pyrrole monomers. In a later stage the charged pyrrole oligomers become highly organophobic due to charged chains and thus migrate in the aqueous phase. Interestingly, during this process they entrap the oleic acid coated carbon nanotubes and transfer them in the water solution. When the chains become sufficiently long and neutral the composite then migrates to the interface. A schematic representation of the different stages of the reaction are shown in Figure 5.

Figure 5.

4. Properties and applications

4.1. Sensors: importance of the fibrillar network

From all the intrinsically conductive polymers, polyaniline appears as the most appealing for numerous applications since it is environmentally safe and air-stable, is water dispersible, can be easily synthesized in bulk quantities, and can react spontaneously with chemical species at room temperature. It is of interest for gas sensing applications [84] because it can be easily processed from an aqueous solution to create thin films with substantial uniformity. These thin films can readily react with redox, protonating or deprotonating agents that will cause immediate changes in the bulk conductivity and the optical properties, i.e. in the optical absorbance spectrum. In general the response of a sensor can be described by the ratio $\Delta R/R_0$, where R_0 and R is the electrical resistance before and after contact between the polymer and the agent that will be detected and $\Delta R = R - R_0$. When the insulating emeraldine base form of the polymer is exposed to HCl or other organic or inorganic acids, a rapid drop in resistance (increase in conductivity), is observed within a short period of time. This doping of polyaniline is achieved by protonation of the imine nitrogens by HCl leading to the emeraldine salt form. The charge created along the backbone by this protonation is counter-balanced by the resulting negatively charged chloride (in the case of HCl) or other counter ions. Consequently, the process is simply an acid-base reaction that can be reversed and the polymer can be re-used.

There are many studies comparing the performance of polypyrrole and polyaniline nanostructures as sensors. As humidity sensors, polyaniline nanorods exhibit negative response values ($R < R_0$) at low humidity levels, whereas polypyrrole nanorods with similar size and shape shows positive response ($R > R_0$). [85] The sensitivity of a

sensor is defined as the slope of the response versus the concentration curve and both polymers demonstrated a linear behavior with sensitivity values of –0.364 for polyaniline and 0.168 for polypyrrole.

The change in conductivity is brought about by the formation of polarons (they can be considered as radical cations) that travel along the polymer backbone. [86] Polarons and bi-polarons are charge carriers in emeraldine salt, which move along the polymer chain upon application of electric field and are responsible for the electrical conductivity of the polymer as evidenced by EPR studies. [87] All these acid-base reactions are completely reversible, something that is essential for a chemical sensor. In addition to the emeraldine salt and base forms, polyaniline can exist in several different oxidation states, including the fully reduced leucoemeraldine form, the half oxidized emeraldine form, and the fully oxidized pernigraniline form (Figure 8b). The oxidation states can either be controlled by synthetic conditions or from subsequent oxidation-reduction reactions. For example, hydrazine is known to convert the emeraldine form to the leucoemeraldine form and thus efficient hydrazine detectors have been developed. [88]

Although much work has been performed on the conductive emeraldine salt form of polyaniline exposed to basic molecules like ammonia gas [89-90] less work has been focused on the use of the insulating emeraldine base form of polyaniline as a sensor for acidic gases such as HCl. This process would be very important and give insight to new applications since there are many fields in which measuring the acid content and concentration is important. A non-trivial example is the rocket launch. HCl is contained

in the exhaust plume of rocket motors that use ammonium perchlorate as the rocket propellant and hydrochloric acid vapors are produced.

The Kaner group pioneered the progress on polyaniline nanofibers as sensing materials for acids, bases, reducing agents, organic vapors, and alcohols. [86; 88] Thin films of both nanofibers and of standard polyaniline have been compared in order to evaluate the response time and sensitivity of the nanofibers relative to films of polyaniline (Figure 7). The changes in electrical resistance were monitored as a function of time as the materials are exposed in various different gases: hydrochloric acid (HCl), ammonia (NH_3), hydrazine (N_2H_4), chloroform ($CHCl_3$), and methanol (CH_3OH). Each gas produces a different response mechanism consisting of various effects on the polyaniline, like protonation, deprotonation, reduction, swelling, and conformational alignment, respectively. The crucial point that demonstrated the importance of the formation of ultra-small nanofibers was that the response time and extent of response was significantly better for thin films composed of polyaniline nanofibers than the values observed for spherical, conventional, particles produced with a common one-phase polymerization process. A high surface area ratio and a porous structure give rise to this phenomenon. The porous structure is the key parameter that enables the easy and rapid diffusion of gases through the film. The small diameter of the nanofibers and the narrow size distribution lead to rapid diffusion of dopants inside the polymer chains. All of these factors explain the observation that the nanofibers give faster and larger responses to dopant exposure as compared to films. Systematic film thickness studies showed no difference in the response magnitude and time (Figure 6).

Figure 6.

Polyaniline and its composites have been widely studied as sensor materials for ammonia. When exposed to ammonia, deprotonation occurs and the conductivity changes since there is a change in the structure from the conducting emeraldine salt to the insulating emeraldine base form. [90a] Previous works on ammonia sensors reported relatively slow response times and small changes in conductivity upon exposure. The study of these systems also showed that as the polymer film thickness is increased, the response to NH_3 is reduced both in sensitivity and time of response [88b] and that a large amount of base is required to convert fully doped polyaniline to the insulating form. This is because fewer dopants are required to reach the percolation threshold for conductivity than those needed to be removed to convert the polymer to be converted to the insulating form. Since the product of the reaction of ammonia and HCl, i.e., NH_4Cl, is not neutral, in the presence of any small amount of water vapor, it will hydrolyze to reform HCl and consequently re-dope the polymer chain thus diminishing the effectiveness of the sensor. With respect to the above, the film is less sensitive and takes longer to respond to a gas-phase base than to an acid. A number of factors, like porosity, surface area, and morphology of the films can explain why the conventional films also respond more slowly to base dedoping than the nanofibers. The larger surface area of the nanofiber films and the smaller diameter gives a shorter response time due to a faster diffusion into the small diameter cylinders.

Recent developments of conductive composite materials involve the incorporation of polyaniline in cellulose paper for the synthesis of highly efficient sensors by exploiting the pH changes upon exposure to acid or bases. Souza and coworkers used polyaniline in order to modify sheets of pressed cellulose fibers, obtained from Eucalyptus grandis and

E.urophylla. [91] In their process the polymer was synthesized and dispersed in chloroform in the first stage. Later on, cellulose sheets were modified with polyaniline particles. The final product can be used to detect the concentration of acidic species in liquid and gaseous solutions through colorimetric analysis. [92] Other gases that can be detected with nanofibers include nitrogen oxides, e.g. NO_2, with the resistivity of the polymer to constantly increase upon exposure to the gas. [93] At this point, we have to mention that polypyrrole nanofibers that have shown excellent response towards ammonia, they showed no response against nitric dioxide (NO_2) even at concentration as high as 100 ppm, a crucial selectivity difference compared to polyaniline. [94]

4.2. Single crystalline polymers: ordering of polyaniline chains

Conductive polymer macromolecular chains are usually forming relatively amorphous or in the best case scenario, semi-crystalline structures. The expected symmetries are located in $2\theta=19$ and 25^o (d spacing=3.5 Å) as observed in XRD powder diffraction pattern and are ascribed to the periodicity parallel and perpendicular to the polymer chains of polyaniline, respectively. [95] This means that either a long range or a short range order can be achieved but in fact the polymer can be considered to be composed of a limited number of ordered and crystalline “islands” embedded in a large amorphous “sea”. This picture represents a semi-crystalline state and systematic study on the reaction conditions needs to be performed for the realization of the optimum properties of these unconventional polymers. [96]

A major advancement in the field is the synthesis for the first time of single crystalline nanoneedles of polyaniline, polypyrrole and Poly (3,4-

ethylenedioxythiophene) (PEDOT) through an interfacial polymerization process. [97] An interfacial polymerization at the liquid/liquid interface allowed these polymers to form highly ordered single crystalline nanoparticles with a rice-like shape in the dimensions lower than 100 nm for both polymers. The electronic behavior of the crystalline polymeric needles was demonstrated in *I*/*V* curves and the conductance switching was found to be extremely fast in the time scale of milliseconds. [97-98] The reaction procedure involves the diffusion of the EDOT monomer in a water/dichloromethane interface. At the start of the reaction, EDOT is dissolved in dichloromethane and $FeCl_3$ is dissolved in water.

It is interesting to note the high crystallinity of the self-assembled polyaniline nanostructures that were obtained in a study by Park et al. The doping agent was tartaric acid and while in reaction time of less than 15 minutes the product was mostly irregularly shaped particles, with extended reaction elongated crystallite particles were formed. The XRD pattern of the polymer powder was typical of the ES-II type of doped polyaniline. [99] The peaks at 2θ values of: 31.9, 34.1, 23.6, and 52.58, correspond to the faces of (212), (004), and (221), (112), and (400) of the ES-II form. From the Bragg equation the d-spacing is 0.2083, 0.2627, 0.3767, and 0.1742 nm, respectively. It is well known that polyaniline obtained from most synthetic procedures is a semicrystalline polymer. The values for degree of crystallinity reported in the literature are commonly less than 50% [100] although there are reports for up to 65%. [101] The nanorods prepared in this study [99] exhibited an unusually high crystallinity, according to the analysis by the authors in the level of >95%. This remarkable crystallinity is the highest reported in the literature

[102] and the lines of the XRD pattern are much narrower than those reported by Dallas et al and Lee et al that will be discussed in the following chapter.

Polymer crystallinity and crystal structure are strongly dependent on the formation kinetics of the nanoparticles. The fast growth of a polymer results in disordered and random orientation of polymer chains and to an amorphous polymer structure. Since the polymerization at the oil/water interface is a relatively slow procedure this has been proven to be favorable for the macromolecules to orient themselves in a hierarchical way. As a result, a one-dimensional nanorod or fiber of high crystallinity can be obtained. This is an important factor since it has been repeatedly demonstrated that high crystallinity and ordered packing of the macromolecules will result in high conductivity and faster response times under exposure in gases. [103]

4.3. Electronic and magnetic properties

4.3.1. Transport mechanism

The extraordinary and novel electrical properties of conductive polymers was something completely unexpected for organic materials, with the exception of graphite. By the late 1970s it was discovered that the conductivity of polyacetylene can increase by a factor of 10^{12} when it is doped with either an electron acceptor like AsF_5 or iodine or an electron donor such as an alkali metal ion. For this polymer the saturation doping level with I_3^- dopant ions is approximately 8 % of the number of carbon atom. [104] The conductivity of the trans isomer of the polyacetylene after doping was found to reach the extraordinary level of 10^4 S/cm. The importance of this discovery resulted to the nomination of the Nobel Prize in Chemistry in 2000 to Prof. Hideki Sirakawa, Prof.Alan J.Heeger and Prof. Alan MacDiarmid. Even if the conductivity values are lower than

conventional metals like copper or silver, they are significantly higher than other polymers and plastics providing new perspectives for the polymer chemistry and physics and its applications (Figure 7a).

Figure 7.

As such, most efforts in the field were focused on the synthesis of either highly conductive polymers or polymers with a metallic-like behavior, i.e. the conductivity is increasing as the temperature is decreasing. In most cases the conductivity reaches a maximum value in a specific temperature where a metal-insulator transition takes place, something that is expected for 1-D conductors due to their intrinsic Peierls instability (due to electron-lattice coupling). [105] The conductivity of a conductive polymer depends on both its ability to transport charge carriers along the macromolecular aromatic backbone and of the carriers to hop between adjacent polymer chains. It is a function of both intra-chain and inter-chain transitions. Since the mechanism involves electron hopping alongside the polymer chains, it is expected that the conductivity will vary according to the specific ordering of the chains, the dimensions of the network and the bridges and connections between the polymer chains and particles. The symmetry of the polymer packing, potential pi-pi stacking and the ordering of the macromolecular chains are crucial in order to facilitate the charge transfer.

In general the four most important factors which influence the conductivity are:

(i) Molecular weight;

(ii) Percentage of crystallinity and inter-chain distance and interactions;

(iii) Oxidation level of the backbone and molecular arrangement;

(iv) Percentage of doping and type of dopant. [107] Specific dopants like camphorsulfonic acid seems favorable;

We will briefly analyze the mechanism that underlines the influence of these factors in the conductivity of the polymers. The crystallinity and pi-pi stacking between adjacent macromolecular chains leads to higher electron delocalization and thus it is expected to facilitate the charge transport. The conjugation further stabilizes the π electrons and drops the energy levels and the energy band gap. Still these materials essentially resemble the inorganic semiconductors where the conductivity increases by introducing an oxidizing or reducing agent, a dopant, that either creates holes which are positive charge carriers or adds electrons near the LUMO levels. In polymers, the charge transports is dominated by a hopping mechanism from domain to domain. Since they are considered as semi-crystalline materials, with the largest domains to be located in the crystalline region. [108a]

The acid doping in the polyaniline backbone takes place on the formerly unprotonated —N= site and the conductivity massively increases despite the unchanged electron concentration. This process results to the formation of polaron bands which are not fully occupied thus allowing intra band transitions with low energy in the NIR region. The formation of this polaron band results in the characteristic three band UV-Visible spectrum (Figure 7c). [108b] Among the doping agents that have been utilized in polyaniline, the camphorsulfonic acid has demonstrated the highest conductivity values compared with other acids. Furthermore the solvent from which the polyaniline is cast results to different chains conformation and to different conductivities. [108] In general,

specific surfactants seem to lead to higher crystallinity and more homogenous morphology. This changes the electronic transport from an activation energy limited process to a more metallic behavior. [109] Polypyrrole is following a similar trend with polyaniline, with the conductivity differences to be in many orders of magnitude depending on the dopant [109b]. For example, p-toluenesulfonic acid has been reported to give conductivity in the range 200-230 S/cm while dodecylbenzenesulfronic acid (DBSA) is significantly lower, at 0.1 S/cm.

4.3.2. Metallic polyaniline

In a previous work concerning the interfacial polymerization of aniline, we obtained needle shaped polyaniline nanoneedles with increased ordering and ultra-small dimensions that demonstrated a very interesting electronic transport behavior. Interestingly, the resistance from 330 to 230 K followed a metallic behavior, with the maximum conductivity value to be 3.5 S/cm. [110] A pi-pi electron overlap amongst the adjacent chains was evidenced by the symmetry at 2θ=25.5 (d spacing=3.5 Å) typical from densely packed phenyl rings. This was observed at the XRD pattern of the polymer powder. A cross-link among the nanoneedles was demonstrated by the SEM images (Figure 4). However, all 1-D conductors as we have previously mentioned are intrinsically unstable and usually a metal-insulator transition occurs at 230 K. [111] In order to study in more detail the electrical behavior of the conductive polyaniline the resistance values in the semiconducting region where plotted according to the Mott relation: $\ln(RT/R330)$ vs $1/T^{1/2}$. This relation is typical in studying semiconductors in a wide temperature range. [112-113] The fitting of the resistance with the relation gave an

excellent linear plot so the polymer can be considered as 1-D conductor (x~ 1/2). The Mott temperature, reflecting the energy required for charge hopping, is derived from the slope and it is calculated to be $1.5 \cdot 10^4$ K.

The work by Lee et al [114] should be highlighted since it presents an undoubtedly groundbreaking work in the field of conductive polymers. Polyaniline with metallic behavior even in the lower temperatures was clearly identified, the first reference for purely and intrinsically metallic polymer. A two-phase synthesis was employed for the synthesis of polyaniline doped with camphor sulfonic acid and an extensive pi-pi stacking was identified from the XRD patterns. Reflectance and dielectric spectra gave an excellent fit with the Drude model. A plasma frequency of 10.500 cm^{-1} (1.3 eV) and a very high conductivity of 1100 S/cm was calculated and a Hagen-Rubens approximation provided an excellent fit for the data (Figure 8). The equations for the Hagen-Rubens and Drude model are given in Figure 8 next to each measurement. As a comparison, single wall carbon nanotubes show a plasma edge of 2000 cm^{-1} and an HR approximation is giving a conductivity between 60 and 170 S/cm. [114c]

In the polyaniline nanoneedles, the metal-insulator transition was monitored through the gradient changes of the magnetic behavior either by altering the temperature (M vs T) or by applying an external magnetic field and obtaining a hysteresis curve (M vs H). For example, in high temperature where the electronic transport was metallic the magnetic measurements indicated a diamagnetic behavior while in lowering the temperature and blocking the spins on the chains, the polymer was paramagnetic. These changes and the correlation between transport and magnetic behavior in a broad temperature range are displayed in the phase diagram of Figure 9. This was assigned to

an electron delocalization in high temperatures that head to the metallic behavior, as it is the case with common metals, while in low temperatures the spins were frozen and the order-disorder transition lead to a paramagnetic behavior. Interestingly, a similar connection of ordering and electron delocalization with high temperature diamagnetism and a disordered phase with low temperature paramagnetism has been recently observed in graphite filaments [115-117]. Especially, graphene has been considered to be a strongly diamagnetic material from recent studies [118]. In the case of these graphitic nanostructures, the high diamagnetic susceptibility is also assigned to an increased ordering and consequently to an electron delocalization and p electrons overlap. This can be correlated with the weakly diamagnetic behavior of aromatic molecules and fullerenes. [116]

Figure 9.

4.4. Energy applications: Composite anode catalysts, self-assembled monolayers and capacitive storage

Intermetallic nanoparticles based on a noble metal and a transitions metal have shown excellent catalytic activity towards methanol oxidation and as fuel cells electrodes. [119] Examples include the platinum based, NiPt, FePt and $FePt_3$ intermetallic alloys. [120] Incorporation of carbon particles, like the commercially available Vulcan XC-72 [121] and other carbon nanomaterials as catalyst support are enhancing the efficiency of direct methanol fuel cells (DMFC). However, the rate of methanol electro oxidation is low. This has been assigned to the low platinum utilization on this conventional carbon support, which is related to the low electrochemically accessible surface area for the deposition of the catalyst Pt particles. Conductive polymers have been proposed as

candidates for a new type of support due to their highly accessible surface area, high conductance and stability, and have even been utilized alongside fullerene buckyballs that are considered very efficient electron acceptors and can attach on the surface of noble metal nanoparticles [122].

Zhao et al developed an *in situ* interfacial polymerization of pyrrole on carbon black and following co-deposition of Pt and Fe on polypyrrole–carbon support in order to prepare a bimetallic Pt-Fe/polypyrrole–carbon catalyst. [123] The Pt–Fe/polypyrole–carbon catalyst demonstrated an improved catalytic activity towards methanol oxidation compared to commercial Pt/C catalyst. We will briefly describe the experimental route for a catalyst with a weight ratio Pt/Fe of 2.5:1: the previously mentioned Vulcan XC-72 carbon black was firstly treated with HNO_3 at 100 °C. This treatment is leading to the formation of hydroxyl and carboxyl groups on the surface of the carbon and it is a known process for solubilizing graphitic materials. In the next step, the PPy–carbon support was synthesized by an *in situ* interfacial method: pyrrole was added in chloroform and carbon was homogeneously dispersed in 100 ml isopropanol–water (volume ratio 1:4) solution with $Fe(NO_3)_3 \cdot 9H_2O$ also dissolved in the suspension. [123]

Self-assembled monolayers of polyaniline on substrates has also been synthesized through a two-phase route. Sawall et al reported an interfacial polymerization technique to form a two-dimensional array of polyaniline fibers grafted to a gold surface using self-assembled monolayer of 4-aminothiolphenol. The process involves firstly the formation a self-assembled monolayer (SAM) of 4-ATP, this was created on an Au surface through the well-known sulfur-gold bond, typical for noble metals and thiol. After this step, the polyaniline nanofibers are directly synthesized onto the Au surface by placing the

substrate at the interface of a biphasic solution of dopant and aniline monomer. The objective of the SAM formation step is to functionalize the Au surface with an amine that will promote the subsequent covalent attachment of the polymer during its formation (*in situ*). During the polymerization, the 4-ATP treated substrate was placed on the interface with the amine groups exposed towards the solution and parallel arranged. Aniline monomers are diffused from the organic layer (bottom) to the interface, then they are protonated by the acidic aqueous layer to form an anilinium cation that subsequently connects to the end of a growing oligomer. [124]

As we have previously discussed nanofibers are having accessible surface areas and present numerous advantages compared to conventional polymers. This could be potentially utilized in order to improve capacitive charge storage applications. Extensive studies towards this directions demonstrated an increase of the capacitance of nanofibers as their diameter decreases. Manohar et al reported a value of 277 F/g that was observed for polyaniline-AMPSA (AMPSA stands for 2-acryloamino-2-methyl-1-propanesulfonic acid) nanofibers of average diameter 23 nm, in aq. 1.0 M CSA electrolyte in the potential range and 0.4–0.5 V (these values are versus SCE). The authors chose this specific range because it lies in the valley between the two redox peaks in the cyclic voltammogram. In contrast non-fibrillar polyaniline·AMPSA powder obtained from the same batch of polyaniline·AMPSA nanofibers using the dedoping/doping procedure yielded a specific capacitance of 11 F/g. From this work it was demonstrated that a fibrillar morphology of the polymer not only leads to significantly higher overall capacitance but also greater symmetry in the charge discharge cycles. The authors estimated the capacitance values using the cyclic voltammetry plots. The unusually high capacitance of

polyaniline·AMPSA composite could also be related to other factors that need to be taken into consideration to further explain these findings. AMPSA is a reactive doping agent and undergoes free radical polymerization in aqueous oxidative conditions. An oxidative environment is a typical environment for the formation of conductive polymers. So, under the conditions of the polymerization, poly-AMPSA may be formed as a byproduct and can increase the available surface area. [125]

High performance asymmetric supercapacitors (*ASC*) have been reported by Shen et al by utilizing the interfacial polymerization of aniline. [126] Aniline was dissolved in dichloromethane and sulfonated graphene in a water/isopropanol mixture. The method lead to excellent interfacial contact between polyaniline nanorods, sulfonated graphene nanosheets and multi-walled carbon nanotubes and to an enhanced cycling performance of the ASC.

In the systems that we discussed till now, small organic acids and hydrochloric acid has been used as doping agents in the polymer backbone. To further expand the gallery of counterbalancing ions, Iekha et al reported the use of polyoxometalates (*POMs*) as doping agents in polyaniline. POMs are considered to increase the homogenous charge separation on the polymer chain by the delocalization of their negative charges and thus facilitate the electron hopping and the charge transfer between the polymer chains. [127-129] When conductive polymers are utilized as electrodes they give rise to pseudocapacitance, to that end, polypyrrole doped with POMs has been utilized as supercapacitors by White et al. [129] and their findings suggested that the highest specific capacitance, energy and power values were with electrodes incorporating polypyrrole doped with 10-molybdo-2-vanadophosphoric acid. Furthermore, polyaniline

nanotubes and nanofibers synthesized through template methods has also lead to good electrochemical performance of lithium batteries and supercapacitors. [130-131] In the field of composite materials hierarchically ordered graphene oxide-polyaniline assemblies have been demonstrated [132] to exhibit a high specific capacitance of 1095 F g^{-1} at 1 A g^{-1}, an energy density of 24.3 W h kg^{-1} and a maximum power density of 28.1 kW kg^{-1} outperforming other solid-state supercapacitors. [133] The authors assigned this improvement to the synergistic effects of the two components, polypyrrole and graphene, in a superior, hierarchical structure of the nanocomposite. A schematic representation of the synthetic procedure is given in Figure 10.

Figure 10.

5. Outlook and perspectives

The long history of the charge and mass transfer through the interface of immiscible liquids provided valuable insights for the recent advances on the challenging field of the self-assembly of nanoparticles on an interface and the generation of conductive polymer nanostructures from two-phase systems. Interfacial polymerization of conductive polymers has been proven a powerful tool for the construction of ultra-small, high quality and crystallinity nanofibers and nanoneedles with superior sensor properties, potential nanoelectronics and energy storage applications and as a powerful method for the synthesis of composite materials. [134] Besides the technological applications and the interesting properties of the resulting polymers, the reaction provides invaluable insights in the study of the fundamental chemical and physical aspects behind the mass and electron transfer and the evolution of nanostructures in an interface.

In summary, this method presents a number of advantages compared to conventional one phase polymerization as it is the slow reaction rate that leads to highly crystalline polymers, the ability to use both organophilic and hydrophilic surfactants and monomers, thin films formation and synthesis of hierarchically ordered composite materials with carbon nanotubes, graphene or silver nanoparticles. Until now the method has been focused on polyaniline, polypyrrole and PEDOT which are the most commonly used conductive polymers. Besides them, there is a wealth of monomers that can be polymerized or simply form functional oligomers with either oxidative or polycondensation methods [135] at an interface and potentially lead to unique nanostructures [136-137] or thin films with new electrochemical, electrochromic, photoluminescence or photoconductive [138], redox or electronic transport properties. This can open new perspectives and pathways in biomedical engineering [139], polymer chemistry and physics. [140]

References

1. a) Hwang WL, Chen M, Cronin B, Holden MA, Baylay H. Asymmetric droplet interface bilayers. J Am Chem Soc 2008; 130: 5878 b) Eeman M, Deleu M. From biological membranes to biomimetic model membranes. Biotechnol Agron Soc Environ. 2010; 14(4): 719-736
2. Rudiner E. Self-assembly and biomimetics in “Nanoscopic materials: Size dependent phenomena and growth principles” Royal Society of Chemistry; 2014. Chapter 10.
3. Michael D, Benjamin I. Molecular dynamics computer simulations of solvation dynamics at liquid/liquid interfaces. J Chem Phys. 1997; 107: 5684

4. Watarai H, Teramae N, Sawada T (Editors). Interfacial nanochemistry: molecular science and Engineering at liquid-liquid interfaces" Kluwer Academic, 2005, New York
5. Volkov AG, Deamer DW (Editors). Liquid interface theory and methods. CRC Press, Inc, New York, 1996
6. Fermín DJ, Duong HD, Ding Z, Brevet PF, Girault HH. Photoinduced Electron Transfer at Liquid/Liquid Interfaces. Part III. Photoelectrochemical Responses Involving Porphyrin Ion Pairs J Am Chem Soc. 1999; 121: 10203
7. Kong YT, Imabayashi S, Kakiuchi T. Two-Phase Azo-Coupling Reactions Driven by Phase-Boundary Potential Across the Liquid-Liquid Interface J Am Chem Soc. 2000; 122: 8215
8. Amemiya S, Ding Z, Zhou J, Bard AJ. Studies of charge transfer at liquid | liquid interfaces and bilayer lipid membranes by scanning electrochemical microscopy J Electroanal Chem. 2000; 483: 7
9. Uchiyama Y, Kitamori T, Sawada T. Role of the Liquid/Liquid Interface in a Phase-Transfer Catalytic Reaction As Investigated by in Situ Measurements Using the Quasi-Elastic Laser Scattering Method. Langmuir. 2000; 16: 6597
10. Chikama K, Negishi T, Nakatani K. Transfer Mechanism of Dodecyl Sulfate with Methylene Blue across an Oil/Water Interface Studied by Single-Droplet Injection and Microabsorption Methods. Bull.Chem.Soc.Jpn. 2003, 76, 295
11. a) Starks CM Phase-Transfer Catalysis. I. Heterogeneous Reactions Involving Anion Transfer by Quaternary Ammonium and Phosphonium Salts J Am Chem Soc 1971; 93: 195 b) Starks CM, Liotta CL, Halpern M (Editors). *Phase-Transfer Catalysis*; Chapman and Hall: New York, 1994.
12. a) Binder WH. Supramolecular Assembly of Nanoparticles at Liquid–Liquid Interfaces. Angew.Chem.Int.Ed. 2005; 44: 5172 – 5175 b) Russell JT, Lin Y, Boker A, Su L, Carl P, Zettl H, He J, Still K, Tangirala R, Emrick T, Littrell K, Thiyagarajan P, Cookson D, Frey A, Wang Q, Russell TP. Angew Chem 2005; 117: 2472 – 2478; Angew Chem Int Ed. 2005; 44: 2420 – 2426
13. Wittbecker EL, Morgan PW. Interfacial polycondensation I. J Polym Sci Part A: Polym Chem. 1996; 34: 521-529.

14. Torini L, Argillier JF, Zydowicz N. Interfacial Polycondensation Encapsulation in Miniemulsion Macromolecules 2005; 38: 3225-3236
15. Chanda M, Roy SK. Plastic technology handbook. 4th ed. Florida: CRC Press; 2006.
16. Dhumal S, Suresh AK. A comprehensive model for kinetics and development of film structure in interfacial polycondensation Polymer 2009; 50: 5851-5864.
17. Chang TMS. Semipermeable microcapsules Science 1964; 146: 524–5.
18. Green KD, Gill IS, Khan JA, Vulfson EN. Microencapsulation of yeast cells and their use as a biocatalyst in organic solvents Biotechnology and Bioengineering 1996; 49(5): 535–43.
19. Yadav SK, Khilar KC, Suresh AK. Release rates from semi-crystalline polymer microcapsules formed by interfacial polycondensation. J Membr Sci 1997; 125(2): 213–8.
20. Torini L, Argillier JF, Zydowicz N. Interfacial Polycondensation Encapsulation in Miniemulsion Macromolecules 2005; 38(8): 3225–36.
21. Desai NV, Rangarajan R, Rao AV, Garg DK, Ankleshwaria BV, Mehta MH. Preliminary investigation of thin film composite reverse osmosis membranes developed from SAN as support membranes. J Membr Sci 1992; 71: 201–10.
22. Peterson RJ. Composite reverse osmosis and nanofiltration membranes. J Membr Sci 1993; 83(1):81–150.
23. Rao AP, Desai NV, Rangarajan R. Interfacially synthesized thin film composite RO membranes for seawater desalination. J Membr Sci 1997; 124(2):263–72.
24. Jeong BH, Hoek EMV, Yan Y, Subramani A, Huang X, Hurwitz G, Asim K. Ghosha, Jawor A. Interfacial polymerization of thin film nanocomposites: A new concept for reverse osmosis membranes. J Membr Sci 2007; 294(1–2): 1–7.
25. a) Buch PR, Jagan Mohan D, Reddy AVR. Preparation, characterization and chlorine stability of aromatic–cycloaliphatic polyamide thin film composite membranes. J Membr Sci. 2008; 309(1–2): 36–44. b) Barona GNB, Lim J, Choi M, Jung B. Interfacial polymerization of polyamide-aluminosilicate SWNT nanocomposite membranes for reverse osmosis Desalination 2013; 325: 138-147

26. Ghosh AK, Jeong BH, Huang X, Hoek EMV. Impacts of reaction and curing conditions on polyamide composite reverse osmosis membrane properties. J Membr Sci. 2008; 311(1–2):34–45.
27. Moniruzzaman M, Chattopadhyay J, Billups WE, Winey KI. Tuning the Mechanical Properties of SWNT/Nylon 6,10 Composites with Flexible Spacers at the Interface, Nano Letters 2007;7(5):1178–85.
28. Tarameshlou M, Jafari SH, Khonakdar HA, Farmahini-Farahani M, Ahmadian S. Synthesis of exfoliated polyamide 6,6/organically modified montmorillonite nanocomposites by in situ interfacial polymerization. Polymer Composites 2007; 28(6):733–8.
29. Cranmer JH, Tesoro GC, Uhlmann DR. Chemical modification of carbon fiber surfaces with organic polymer coatings. Ind.Eng.Chem.Prod.Res.Dev. 1982; 21(2):185–90.
30. Salehi-Mobarakeh H, Ait-Kadi A, Brisson J. Improvement of mechanical properties of composites through polyamide grafting onto kevlar fibers. Pol.Eng.Sci. 1996; 36(6): 778–85.
31. Hisamoto H, Shimizu Y, Uchiyama K, Tokeshi M, Kikutani Y, Hibara A, et al. Chemicofunctional Membrane for Integrated Chemical Processes on a Microchip Anal Chem 2003; 75(2): 350–4.
32. De Jong J, Lammertink RG, Wessling M. Membranes and microfluidics: a review. Lab on a Chip 2006; 6(9):1125–39.
33. Aleshin AA. Polymer Nanofibers and Nanotubes: Charge Transport and Device Applications. Adv Mater 2006; 18: 1727.
34. Kohlman, RS, Epstein AJ. *Handbook of Conducting Polymers*, 2nd ed.; Marcel Dekker: New York, 1998
35. Pringsheim E, Zimin D, Wolfbeis OS. Fluorescent Beads Coated with Polyaniline: A Novel Nanomaterial for Optical Sensing of pH Adv. Mater. 2001; 13: 819-822.
36. a) Sukeerthi S, Contractor AQ. Anal. Chem. *Molecular Sensors and Sensor Arrays Based on Polyaniline Microtubules* 1999; 71: 2231-2236. b) Bossi A,

Piletsky SA, Piletska EV, Righetti PG, Turner APF. An Assay for Ascorbic Acid Based on Polyaniline-Coated Microplates Anal Chem 2000; 72: 4296-4300.

37. Janata J, Josowicz M. Conducting polymers in electronic chemical sensors. Nat.Mater. 2003; 2: 19-24.
38. a) Lin Y, Skaff H, Emrick T, Dinsmore AD, Russell AT. Nanoparticle Assembly and Transport at Liquid-Liquid Interfaces Science 2003; 299: 226 b) Chevalier Y, Bolzinger MA Emulsions stabilized with solid nanoparticles: Pickering emulsions Coll Surf A. Physicochemical and engineering aspects 2013; 439: 23-34
39. Samec Z. Electrical double layer at the interface between two immiscible electrolyte solutions Chem.Rev. 1988; 88: 617
40. Ishizaka S, Kim HB, Kitamura N. Time-Resolved Total Internal Reflection Fluorometry Study on Polarity at a Liquid/Liquid Interface Anal Chem. 2001; 73: 2421
41. Boguslavsky LI, Volkov AG. in V.E.Kazarinov. (Editor) The Interface Structure and Electrochemical Processes at the Boundary between Two Immiscible Liquids. Springer, Berlin
42. Tauer K, Kozempel S, Rother G. The interface engine: Experimental consequences J Coll Int Sci. 2007;312:432-438
43. Bessho K, Uchida T, Yamauchi A, Shioya T, Teramae N. Microenvironments of 8-anilino-1-naphthalenesulfonate at the heptane-water interface: time-resolved total internal reflection fluorescence spectroscopy Chem Phys Lett. 1997; 264: 381
44. a) Ishizaka S, Kitamura N. Time-Resolved Total Internal Reflection Fluorometry Study on Chemical and Structural Characteristics at Water/Oil Interfaces Bull Chem Soc Jpn 2001; 74: 1983 b) Wang H, Borquet E, Eisenthal KB Generalized interface polarity scale based on second harmonic spectroscopy J Phys Chem B 1998; 102: 4927-4932
45. Bakeeva LE, Grinius LL, Jasaitis AA, Kuliene VV, Levitsky DO, Liberman EA, Severina II, Skulachev VP. Conversion of biomembrane-produced energy into electric form. II. Intact mitochondria. BBA-Bioenergetics 1970; 216(1): 13-21

46. Samec Z, Mareček V, Weber J. Charge Transfer between Two Immiscible Electrolyte Solutions. Part IV. Electron Transfer between Hexacyanoferrate (III) in Water and Ferrocene in Nitrobenzene Investigated by Cyclic Voltammetry with Four-Electrode System. J Electroanal Chem. 1979; 103: 11
47. a) Rao CNR, Kalyanikutty KP. The Liquid–Liquid Interface as a Medium To Generate Nanocrystalline Films of Inorganic Materials Acc Chem Res. 2008; 41(4): 489-499 b) Reymond F, Fermin D, Lee HJ, Girault HH. Electrochemistry at liquid/liquid interfaces: methodology and potential applications. Electrochimica Acta 2000; 45: 2647-2662 c) Volkov A (Editor) Interfacial catalysis CRC Press. 2002. d) Lee HJ, Beattie PD, Seddon BJ, Osborne MD, Girault HH. Amperometric ion sensors based on laser-patterned composite polymer membranes J. Electroanal. Chem. 1973; 440: 73
48. Rabinowitch E, Weiss J. Reversible oxidation of chlorophyll Proc Royal Soc B. 1937; 124:277
49. Ishizaka S, Nishijima Y, Kitamura N. A thermodynamic study on the complexation between riboflavin and a diaminotriazine derivative mediated by triple hydrogen bonds at water/oil interfaces Anal Bioanal Chem. 2006; 386: 749–758
50. a) Nochi K, Yamaguchi A, Hayashita T, Uchida T, Teramae N. Direct Observation of Alkali Metal Ion Recognition Processes at the Heptane/Water Interface by Second Harmonic Generation Spectroscopy J Phys Chem B 2002; 106: 9906-9911 b) Srivastava S, Nykypanchuk D, Fukuto M, Halverson JD, Tkachenko AV, Yager KG, Gang O Two-dimensional DNA-programmable assembly of nanoparticles at liquid interfaces J Am Chem Soc 2014; 136: 8323-8332 c) Sanyal MK, Agrawal VV, Bera MK, Kalyanikutty KP, Daillant J, Blot C, Kubowisz S, Konovalov O, Rao CNR Formation and ordering of gold nanoparticles at the toluene-water interface J Phys Chem C. 2008; 112: 1739-1743 d) Srivastava S, Nykypanchuk D, Fukuto M, Gang O. Tunable Nanoparticle Arrays at Charged Interfaces ACS Nano 2014; 8(10): 9857-9866
51. a) Volkov AG, Deamer DW. Redox chemistry at liquid/liquid interfaces Progr Colloid Polym Sci. 1997; 103: 21-28 b) Myers D Liquid-fluid interfaces.

Surfaces, Interfaces, and Colloids: Principles and Applications, Second Edition. 1999 John Wiley & Sons, Inc. Chapter 8.

52. a) Garbassi F, Morra M, Occhiello E. “Polymer Surfaces: from physics to technology” John Wiley & Sons 1994 b) Triezenberg DG, Zwanzig R. Phys Rev Lett 1972; 28: 1183 c) Rey AD. Langmuir 2006; 22: 3491-3493
53. Fisk S, Widom B. Structure and Free Energy of the Interface between Fluid Phases in Equilibrium near the Critical Point J Chem Phys 1969; 50: 3219
54. Yang AJM, Fleming PD, Gibbs JH. Molecular theory of surface tension J Chem Phys. 1976; 64: 3732
55. Aarts DGAL, Schmidt M, Lekkerkerker HNW, Mecke KR. Microscopy on Thermal Capillary Waves in Demixed Colloid-Polymer Systems. Adv in Solid State Phys. 2005; 45: 15–27
56. Aarts DGAL, Schmidt M, Lekkerkerker HNW. Direct Visual Observation of Thermal Capillary Waves Science 2004; 304: 847
57. a) Fowkes FM. Determination of interfacial tensions, contact angles, and dispersion forces in surfaces by assuming additivity of intermolecular interactions in surfaces. J Phys Chem. 1962; 66: 382 b) Marchand A, Weijs JH, Snoeijer JH, Andreotti B. Why is surface tension a force parallel to the interface? Am J Phys 2011; 79:999 c) Bulou J, Raynal JM, Vial J. An Interfacial Tension Treatment with an Improved Good-Girifalco Equation Using Solubility Parameters J Coll Int Sci 1984; 98: 168
58. D’Arcy JM, Tran HD, Tung VC, Tucker-Schwartz AK, Wong RP, Yang Y, Kaner RB. Versatile solution for growing thin films of conducting polymers. Proc Nat Acad Sci 2010; 107: 19673.
59. a) Binks BP, Clint JH, Fletcher PDI, Lees TJG, Taylor P. Growth of Gold Nanoparticle Films Driven by the Coalescence of Particle-Stabilized Emulsion Drops Langmuir 2006; 22: 4100-4103 b) Chengara A, Nikolov AD, Wasan DT, Trokhymchuk A, Henderson D. Spreading of nanofluids driven by the structural disjoining pressure gradient J Colloid Interf. Sci. 2004; 280: 192-201
60. Huang J, Kaner RB. The intrinsic nanofibrillar morphology of polyaniline Chem Commun**.** 2006; 367

61. Mulchandani A, Myung NV. Conducting polymer nanowires-based label free-biosensors. Curr Opin Biotechnol 2011; 502-508
62. Huang J, Kaner RB. Nanofiber formation in the chemical polymerization of aniline: a mechanistic study. Angew Chem Int Ed. 2004; 43: 5817 –5821
63. a) Huang J, Kaner RB. A general chemical route for polyaniline nanofibers. J Am Chem Soc. 2004; 126: 851-855 b) Li D, Huang J, Kaner RB Polyaniline nanofibers: a unique polymer nanostructure for versatile applications Acc Chem Res 2009; 42(1): 133-145
64. Chen J, Chao D, Lu X**,** Zhang W. Novel interfacial polymerization for radially oriented polyaniline nanofibers. Mater Lett**.** 2007; 61(6): 1419-1423
65. a) Li W, Zhang Q, Chen D, Li L. Study of nanofibers of polyaniline via interfacial polymerization J Macromol Sci Part A. 2006; 43(11): 1815 – 1824 b) Gao H, Jiang T, Han B, Wang Y, Du J, Liu Z, Zhang J. Aqueous/ionic liquid interfacial polymerization for preparing polyaniline nanoparticles Polymer 2004; 45(9): 3017-3019 c) He Y**.** One dimensional polyaniline nanostructures synthesized by interfacial polymerization in a solid stabilized emulsion. Appl. Surf. Sci. 2006; 252(6): 2115-2118
66. a) Su K, Nuraje N, Zhang L, Chu IW, Matsui H, Yang NL. First Preparations and Characterization of Conductive Polymer Crystalline Nanoneedles. Macromol Symp. 2009; 279: 1–6 b) Zhang L, Waterhouse GIN, Zhang L. Journal of Nanomaterials. 2011 http://dx.doi.org/10.1155/2011/467170
67. Tran HD, D'Arcy JM, Wang Y, Beltramo PJ, Strong VA, Kaner RB. The oxidation of aniline to produce polyaniline: a process yielding many different nanoscale structures. J Mater Chem. 2011; 21: 3534-3550
68. Zhang J, Mandler D, Unwin PR. Interfacial polymerisation of anilinium at Langmuir monolayers. Chem Commun**.** 2004, 450-451.
69. Liu S, Zhu K, Zhang Y, Xu J. Cyclic polyaniline nanostructures from aqueous/organic interfacial polymerization induced by polyacrylic acid. Polymer 2006; 47(22): 7680-7683
70. a) Li J, Jia Q, Zhu J, Zheng M. Interfacial polymerization of morphologically modified polyaniline: from hollow microspheres to nanowires Polym Int 2008;

57:337–341 b) Neugebauer JM. Detergents: An Overview. Meth. Enzymol. 1990; 182: 239-253

71. Xing S, Zheng H, Zhao G. Preparation of polyaniline nanofibers via a novel interfacial polymerization method Synth Met. 2008; 158(1-2): 59-63
72. Ding S, Mao H, Zhang W. Fabrication of DBSA-doped polyaniline nanorods by interfacial polymerization J Appl Polym Sci. 2008; 109: 2842–2847
73. Tat'yana V, Vernitskaya, Efimov ON. Polypyrrole: a conducting polymer; its synthesis, properties and applications Russ Chem Rev 1997; 66: 443
74. Shang S, Zeng W, Tao X. Fabrication of conducting polypyrrole- β-cyclodextrin nano- and micro-spheres using molecular templates RSC Adv. 2012; 2: 4675
75. Lee KP, Gopalan AI, Lee SH, Kim MS. Polyaniline and cyclodextrin based chiral nanobundles—functional materials having size and enantioselectivity Nanotechnology 2006; 17**:** 375-380
76. a) Tan Y, Ghandi K. Kinetics and mechanism of pyrrole chemical polymerization Synth.Met. 2013; 175: 183 b) Dallas P, Niarchos D, Vrbanic D, Boukos N, Pejovnik S, Petridis D. Interfacial polymerization of pyrrole and in situ synthesis of silver-ppy nanocomposites Polymer 2007; 48: 2007 b) Stejskal J. Chem Papers 2013; 67 (8): 814–848 c) Simultaneous synthesis of polyaniline nanofibers and metal (Ag and Pt) nanoparticles. Huang LM, Liao WH, Ling HC, Wen TC. Mater Chem Phys. 2009; 116(2-3): 474-478 d) Bedre MD, Basavaraja S, Salwe BD, Shivakumar V, Arunkumar L, Venkataraman A. Preparation and Characterization of Pani and Pani Ag Nanocomposites via Inter-Faci al Polymerization Pol Comp 2009; 30:1668–1677
77. Mukherjee P, Nandi AK. Langmuir 2010; 26: 2785-2890
78. Yang F, Chu Y, Ma S, Zhang Y, Liu J. Preparation of uniform silica/polypyrrole core/shell microspheres and polypyrrole hollow microspheres by the template of modified silica particles using different modified agents J Coll. Interf Sci. 2006; 301: 470
79. a) Zhou H, Sun Y, Li G, Chen S, Lu Y. Interfacial assembly and electrochemical properties of nafion-modified-graphene/polyaniline hollow spheres Polymer 2014; 55(17): 4459–4467 b) Sergio H. Domingues SH, Salvatierra RV, Oliveira

MM, Zarbin AJG. Transparent and conductive thin films of graphene/polyaniline nanocomposites prepared through interfacial polymerization Chem Commun 2011; 47: 2592-2594

80. Tamer U, Kanbes C, Erta N. Branched Fibers of Conducting Polypyrrole: Synthesis and Characterization Int J Pol Anal Char 2009; 14(3): 259 – 270
81. a) Georgakilas V, Dallas P, Niarchos D, Boukos N, Trapalis C. Polypyrrole/MWNT nanocomposites synthesized through interfacial polymerization Synth Met. 2009; 159: 632–636 b) Han Y, Shen M, Lin X, Ding B, Zhang L, Tong H, Zhang X. Ternary phase interfacial polymerization of polypyrrole MWNT nanocomposites with core-shell structure. Synthetic Metal 2012; 162: 753-758
82. Pomposo AJ, Ochoteco E, Pozo C, Carrasco P-M, Grande H-J, Rodrıguez FJ. Polym. Conductivity enhancement in raw polypyrrole and polypyrrole nanoparticle dispersions Adv. Technol. 2006; 17: 26–29
83. Spitalsky Z, Tasis D, Papagelis K, Galiotis C. "Carbon nanotube-polymer composites: chemistry, processing, mechanical and electrical properties Prog Pol Sci. 2010; 35: 357-401
84. Deepshikha A, Basu T. A Review on Synthesis and Characterization of Nanostructured Conducting Polymers (NSCP) and Application in Biosensors Anal Letters 2011; 44: 1126–1171
85. Joulazadeh M, Navarchian AH, Niroomand M. Advances in Polymer Technology A Comparative Study on Humidity Sensing Performances of Polyaniline and Polypyrrole Nanostructures 2014; 33: 21461
86. Huang J, Virji S, Kaner RB, Weiller BH. Nanostructured polyaniline sensors Chem Eur J. 2004; 10: 1314-1319
87. Krinichnyi VI, Tokarev SV, Roth HK, Schrodner M, Wessling B. EPR study of charge transfer in polyaniline highly doped by p-toluenesulfonic acid Synth Met 2006; 156: 1368–1377
88. Virji S, Huang J, Kaner RB, Weiller BH. Polyaniline nanofiber gas sensors: examination of response mechanism. Nano Lett. 2004; 4(3): 491-496
89. Kukla AL, Shirshov YM, Piletsky SA. Sens Act B 1996; *37*: 135-140.

90. a) Wang L, Huang H, Xiao S, Cai D, Liu Y, Liu B, Wang D, Wang C, Li H, Wang Y, Li Q, Want T Enhanced Sensitivity and Stability of Room-Temperature NH_3 Sensors Using Core−Shell CeO_2 Nanoparticles@Cross-linked PANI with p−n Heterojunctions ACS Appl Mater Int. 2014; 6: 14131-14140 b) Wu S, Zeng F, Li F, Zhu Y. Ammonia sensitivity of polyaniline films via emulsion polymerization Eur Polym J. 2000; *36*: 679-683.
91. Souza FG, Oliveira GE, Anzai T, Richa P, Cosme T, Nele M, Rodrigues CHM, Soares BG, Pinto JC. A Sensor for Acid Concentration Based on Cellulose Paper Sheets Modified with Polyaniline Nanoparticles Macromol Mater Eng. 2009; 294: 739–748
92. a) Xia Y, Wiesinger JM, MacDiarmid AG. Chem Mater 1995; 7: 443. b) Davey JM, Too CO, Ralph SF, Maguire LK, Wallace GC. Macromolecules 2000; 33: 7044 c) Huang WS, Humphrey BD, MacDiarmid AG. J Chem Soc Far Trans. 1986; 82: 2385-2400.
93. Yan XB, Han ZJ, Yang Y, Tay BK. NO_2 gas sensing with polyaniline nanofibers synthesized by a facile aqueous/organic interfacial polymerization Sens Act B 2007; 123: 107–113
94. Hernandez SC, Chaudhuri D, Chen W, Myung NV, Mulchandani A. Single Polypyrrole Nanowire Ammonia Gas Sensor Electroanalysis 2007; 19-20: 2125 – 2130
95. a) Moon YB, Cao Y, Smith P, Heeger AJ. *Polym Commun* 1989; 30:196 b) Yang CH, Chih YK, Cheng HE, Chen CH. Nanofibers of self-doped polyaniline *Polymer 2005;* **46**: 10688
96. Detsri E, Dubas ST. Interfacial polymerization and its layer by layer assembly into polyelectrolytes multilayer thin-films. J Appl Pol Sci 2013; 128: 558-565
97. Nuraje N, Su K, Yang NI, Matsui H. Liquid/Liquid Interfacial Polymerization To Grow Single Crystalline Nanoneedles of Various Conducting Polymers ACS Nano. 2008; 2(3): 502
98. Su K, Nuraje N, Zhang L, Chu IW, Peetz RM, Matsui H, Yang NL. Fast Conductance Switching in Single-Crystal Organic Nanoneedles Prepared from an

Interfacial Polymerization-Crystallization of 3,4-Ethylenedioxythiophene Adv Mater. 2007; 19: 669–672.

99. Park MC, Sun Q, Deng Y. Polyaniline microspheres consisting of highly crystallized nanorods Macromol Rapid Comm. 2007; 28: 1237-1242.
100. Pouget JP, Jozefowicz MA, Epstein AJ, Tang X, MacDiarmid AG. X-ray structure of polyaniline Macromolecules 1991; 24: 779.
101. Manim A, Athinarayanasamy K, Kamaraj P. Crystalline order in polyaniline J Mater Sci Lett. 1995; 14: 1594.
102. Zheng W, Angelopoulos M, Epstein AJ, MacDiarmid AG. Concentration Dependence of Aggregation of Polyaniline in NMP Solution and Properties of Resulting Cast Films Macromolecules 1997; 30: 7634.
103. MacDiarmid AG, Epstein AJ Synth Met. Secondary doping in polyaniline 1995; 69: 85.
104. Tsukamoto J. Recent advances in highly conductive polyacetylene Adv Phys 1992; 41: 509
105. Kaiser AB. Electronic transport properties of conducting polymers and carbon nanotubes Rep. Prog. Phys. 2001; 64: 1–49
106. Wei Z, Faul CF. Interfacial polymerization of morphologically modified polyaniline: from hollow microspheres to nanowires Macromol Rapid Commun. 2008; 29: 280–292
107. Su C, Wang G, Huang F, Li X. Effects of synthetic conditions on the structure and electrical properties of polyaniline nanofibers. J Mater Sci. 2008; 43:197–202
108. a) Strobl G. The physics of polymers: concepts for understanding their structure and behavior. Springer-Verlag Berlin Heidelberg 2007 b) Stafstrom S, Bredas JL, Epstein AJ, Woo HS, Tanner DB, Huang WS, MacDiarmid AG. Polaron Lattice in Highly Conducting Polyaniline: Theoretical and Optical Studies Phys Rev Lett. 1987; 59: 1464 c) Stejskal J, Kratochvil P. Polyaniline dispersions 2. UV-Vis absorption spectra Synth Met 1993; 61: 225-231
109. a) Heeger AJ Synth.Met. 1993; 55-57; 4371 b) Nalwa HS Advanced Functional Molecules and Polymers: Volume 3: Electronic and Photonic

Properties: Electronic and Photonic Properties v. 3 Taylor and Francis. 2011; Page 130, Table 15

110. Dallas P, Stamopoulos D, Boukos N, Tzitzios V, Niarchos D, Petridis D. Characterization, magnetic and transport properties of polyaniline synthesized through interfacial polymerization Polymer 2007; 48: 3162

111. a) Unsworth J, Lunn BA, Innis PC, Jin Z, Kaynak A, Booth NG. Technical review: conducting polymer electronics. J Intel Mat Syst Str 1992; 3: 380–395 b) Angelopoulos M. Conducting polymers in microelectrons IBM J Res Dev 2001; 45: 57–75. c) Gospodinova N, Terlemezyan L. Prog Polym Sci Conducting polymers prepared by oxidative polymerization: polyaniline 1998; **23:** 1443–1484. d) Bhadra S, Chattopadhyay S, Singha NK, Khastgir D. Improvement of conductivity of electrochemically synthesized polyaniline J Appl Polym Sci 2008; 108: 57–64.

112. Mott N F and David E A 1979 *Electronic Processes in Non-Crystalline Materials* (Oxford: Oxford University Press)

113. Reghu M, Cao Y, Moses D, Heeger AJ. Counterion-induced processibility of polyaniline: Transport at the metal-insulator boundary Phys Rev B 1993;47:1758

114. a) Lee K, Cho KS, Sung HP, Heeger AJ, Lee CW, Lee SH. Metallic transport in polyaniline *Nature* 2006; 441(1): 65-68 b) Lee SH. Lee DH, Lee K. Lee CW. High-performance polyaniline prepared via polymerization in a self-stabilized dispersion. Adv Funct Mater. 2005; 15: 1495–1500 c) Ruzicka B, Degiorgi L. Optical and dc conductivity study of potassium-doped single-walled carbon nanotube films Phys Rev B. 2000; 61(4): R2468

115. Calderon-Moreno JC, Labarta A, Batlle X, Crespo D, Pol VG, Pol SV, Gedanken A. Magnetic properties of dense graphitics filaments formed via thermal decomposition of mesitylene in an applied electric field. Carbon 2006; 44: 2864

116. a) Johansson MP, Juselius J, Sundholm D. Sphere currents of buckmisterfullerene Angew.Chem.Int.Ed. 2005; 44: 1843 b) Shibayama Y, Sato

H, Enoki T. Disordered Magnetism at the Metal-Insulator Threshold in Nano-Graphite-Based Carbon Materials Phys Rev Lett. 2000; 84(8): 1744

117. Wabayashi K, Fujita M, Ajiki H, Sigrist M. Electronic and magnetic properties of nanographite ribbons Phys Rev B 1999; 59(12): 8271.

118. Kuzemsky AL. Unconventional and Exotic Magnetism in Carbon-Based Structures and Related Materials Int J Mod Physics B. 2013; 27: 1330007

119. Leonard BM, Zhou Q, Wu D, DiSalvo FJ. Facile Synthesis of PtNi Intermetallic Nanoparticles: Influence of Reducing Agent and Precursors on Electrocatalytic Activity Chem Mater. 2011; *23*(5): 1136–1146

120. Wang C, van der Vliet D, More KL, Zaluzec NJ, Peng S, Sun S, Daimon H, Wang G, Greeley J, Pearson J, Paulikas AP, Karapetrov G, Strmcnik D, Markovic NM, Stamenkovitz VR. Multimetallic Au/$FePt_3$ Nanoparticles as Highly Durable Electrocatalyst Nano Lett. 2011; 11: 919-926

121. Wu G, Li L, Li JH, Xu BQ. Polyaniline-carbon composite films as supports of Pt and PtRu particles for methanol electrooxidation Carbon 2005; 43: 2579-2587

122. Bai Z, Yang L, Guo Y, Zheng Z, Hu C, Xu P. High-efficiency palladium catalysts supported on ppy-modified C_{60} for formic acid oxidation. Chem. Commun. 2011; 47: 1752–1754

123. Zhao H, Li L, Yang J, Zhang Y, Li H. Synthesis and characterization of bimetallic Pt–Fe/polypyrrole–carbon catalyst as DMFC anode catalyst Electrochem Commun 2008; 10(6): 876

124. Sawall DD, Villahermosa RM, Lipeles RA, Hopking A, Hopkins R. Interfacial polymerization of polyaniline nanofibers grafted to Au surfaces. Chem. Mater. 2004; 16: 1606-1608

125. Zhang X**,** King RCY, Jose A**,** Manohar SK. Nanofibers of polyaniline synthesized by interfacial polymerization Synth Met**.** 2004; 145(1): 23-29

126. Shen J, Yang C, Li X, Wang G High performance asymmetric supercapacitor based on nanoarchitectured polyaniline/graphene/carbon nanotube and activated graphene electrodes ACS Appl Mater Interf 2013; 5: 8467-8476

127. lekha CP, Subramanian S, Padiyan DP. Paper Investigation of pseudocapacitance effect and frequency dependence of ac impedance in polyaniline–polyoxometalate hybrids J Mater Sci 2009; 44:6040–6053

128. Manivel A, Asiri AM, Alamri KA, Villarreal TL, Anandan S. Interfacially synthesized PAni-PMo12 hybrid material for supercapacitor applications Bull Mater Sci 2014; 37:861

129. White AM, Slade RCT Polymer electrodes doped with heteropolymetallates and their use within solid-state supercapacitors Synth Met 2003; 139:123

130. Pan L, Qiu H, Dou C, Li Y, Pu L, Xu J, Shi Y. Conducting Polymer Nanostructures: Template Synthesis and Applications in Energy Storage Int J Mol Sci. 2010; 11: 2636-2657

131. Wanlu Y, Zan G, Ningning S, Yunya Z, Yingchao Y, Jun W. Synthesis of hollow polyaniline nano-capsules and their supercapacitor application J Power Sources 2014; 272: 915-921

132. Li D, Li Y, Feng Y, Hu W, Feng W. Hierarchical graphene oxide/polyaniline nanocomposites prepared by interfacial electrochemical polymerization for flexible solid-state supercapacitors J Mater Chem A. 2015; 3: 2135-2143

133. Hao QL, Wang HL, Yang XJ, Lu LD, Wang X. Liquid/Liquid Interfacial Polymerization to Fabricate Sulfonated Graphene/Polyaniline Nanocomposite for Supercapacitors Appl Mech Mater 2010; 29-32: 1902-1906

134. Joseph N, Varghese J, Sebastian MT. Self-assembled polyaniline nanofibers with enhanced electromagnetic shielding properties. RSC Adv. 2015; 5: 20459

135. Feng L, Zhu C, Yuan H, Liu L, Lv F, Wang S. Conjugated polymer nanoparticles: preparation, properties, functionalization and biological applications Chem Soc Rev. 2013; 42: 6620--6633

136. Dallas P, Zboril R, Bourlinos AB, Jancik D, Niarchos D, Panacek A, Petridis D. Cornet-like phosphotriazine/diamine polymer as reductant and matrix

for the synthesis of silver nanocomposites with antimicrobial activity Macromol Mater Eng 2010; 295(2): 108

137. Clayden J, Rowbottom SJM, Hutchings MG, Ebenezer WJ. Formation of water-soluble sulfonated azacalix[4]arenes from cyanuric chloride Tetrahedron Lett. 2009; 50: 3923-3925

138. Fried JR. Polymer Science and Technology. Prentice Hall, 2003. Chapter 10 “Engineering and specialty polymers”

139. Chen J, Wang F, Liu Q, Du J. Antibacterial polymeric nanostructures for biomedical applications Chem. Commun. 2014; 50: 14482--14493

140. Chen HF, Yang SJ, Tsai ZH, Hung WY, Wang TC, Wong KT. 1,3,5-Triazine derivatives as new electron transport–type host materials for highly efficient green phosphorescent OLEDs J Mater Chem. 2009; 19: 8112–8118

- Figure captions

Figure 1. The redox reaction in the interface of two immiscible solutions (Phases 1 & 2). In this example the reduced and oxidized species return to the initial phase and no migration to another phase takes place

Figure 2. a) Schematic representation of the interfacial polymerization of aniline demonstrating the formation of charged polyelectrolyte chains. The heavier chloroform phase is at the bottom and the lighter aqueous phase at the top. Persulfate ions ($S_2O_8^{2-}$) and HCl are added in the aqueous phase to initiate the oxidative polymerization. b) The stages of the interfacial polymerization of aniline. Notice that the monomer is in the lower, chloroform phase, but during the course of the reaction diffuses firstly to the interface and then to the aqueous phase, where the dark green emeraldine salt form of polyaniline can be readily disperse. See Tran et al [67]

Figure 3. Ultra-small polyaniline polyaniline nanoneedles synthesized in a water-chloroform system. The polymer is doped with HCl and no surfactants were added during the synthesis. The needles are exhibiting a metal-insulator transition at 230 K and a diamagnetism to paramagnetism transition. By P.Dallas et al. Reproduced from Ref.110 ©: Elsevier. Adapted with permission.

Figure 4. a) The mechanism of the oxidative polymerization of pyrrole. Tan et al [76a] In a typical reaction ferric ions are oxidizing the monomer by attacking the α-position of the pyrrole ring, and the reaction propagates through subsequent addition of pyrrole molecules. b) Schematic representation of the interfacial synthesis of silver/polypyrrole thin films and a characteristic TEM image depicting the formation of silver nanoparticles. By P.Dallas et al. Ref.76b. ©: Elsevier. Adapted with permission.

Figure 5. For the synthesis of polypyrrole/CNT nanocomposites, carbon nanotubes functionalized with oleylamine are entrapped by polypyrrole chains and migrate initially to the aqueous phase and in a second stage to the interface. Due to the insolubility of the polypyrrole macromolecules after the completion of the reaction the nanocomposite is forming an interfacial film. By V.Georgakilas et al. Ref.81a © Adapted with permission.

Figure 6. I) Normalized resistance vs time curves showing the response of polyaniline sensors after exposure to 100 ppm gaseous HCl. Three different nanofiber polyaniline films are presented with the following thicknesses: 0.2 μm (—), 0.4 μm (- - -), 2.0 μm (⋯).Copyright: John Wiley and Sons. By Huang et al, Ref 86. Adapted with permission.

Figure 7. Table: The conductivity of a number of intrinsically conductive polymers relative to common metals and plastics. The values are in S/cm. Scheme: The three oxidation states of polyaniline: (a) a fully reduced leucoemeraldine base (LEB); (b) a fully oxidized pernigraniline base (PNB); and (c) a half oxidized/half reduced emeraldine base (EB) state. Detailed analysis of the conductivity of polymers and nanotubes is provided in the article by Kaiser. [105] For a review on the aniline oligomers structure and oxidation states see the work by Wei et al [106] II. The three optical transitions between the valence, the conduction and the polaron band of the conductive green polyaniline are indicated.

Figure 8. Phase diagram of the nanoneedles synthesized through an interfacial polymerization without the presence of any surfactants. The diagram is representing how the changes of the electronic transport and magnetic behavior are correlated. Please notice the gradient transition from a diamagnetic/metallic state to a paramagnetic/semiconductor-insulator state. By Dallas et al. Reproduced from Ref.110. ©: Elsevier. Adapted with permission.

Figure 9. a) Reflectance spectra with a Hagen-Rubens approximation fitting b) Frequency dependent conductivity, (solid line), theoretical fit by the Drude model (red) and the interchain contribution to the conductivity (blue) c) The real part of the dielectric

function and a fit with the Drude model. The equations for each model are given in the boxes next to each graph. Reprinted by permission from Macmillan Publishers Ltd: Nature, Ref 114a, © 2006

Figure 10. A schematic representation of the preparation of hierarchically ordered graphene oxide/polyaniline nanocomposites by interfacial electrochemical polymerization. By Li et al [131]. © Royal Society of Chemistry. Adapted with permission.

- **Figures**

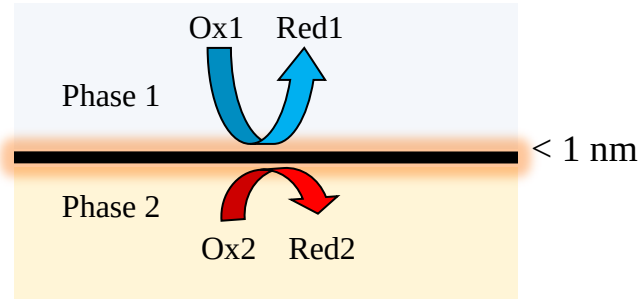

Figure 1.

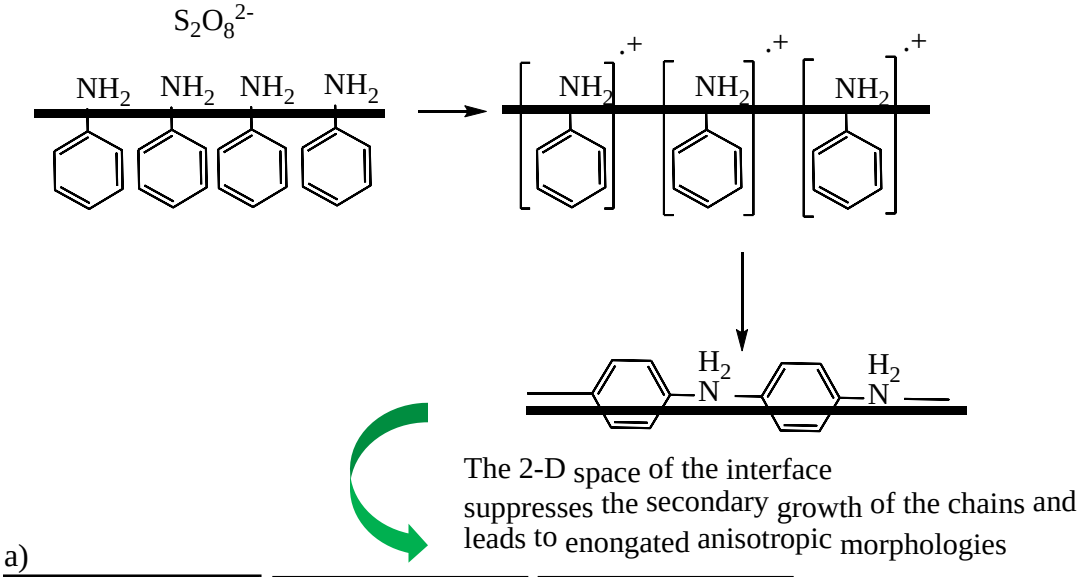
$S_2O_8^{2-}$
NH_2 NH_2 NH_2 NH_2
NH_2 NH_2 NH_2
H_2N H_2N
The 2-D space of the interface suppresses the secondary growth of the chains and leads to enongated anisotropic morphologies

a)

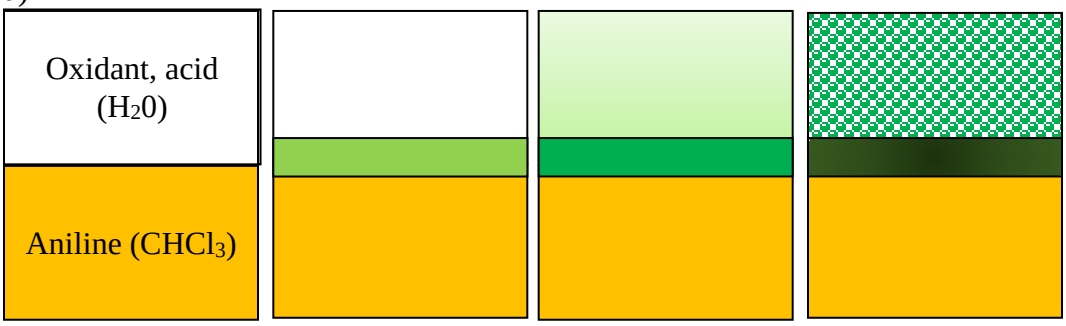
Oxidant, acid (H_20)
Aniline ($CHCl_3$)

b)

Figure 2.

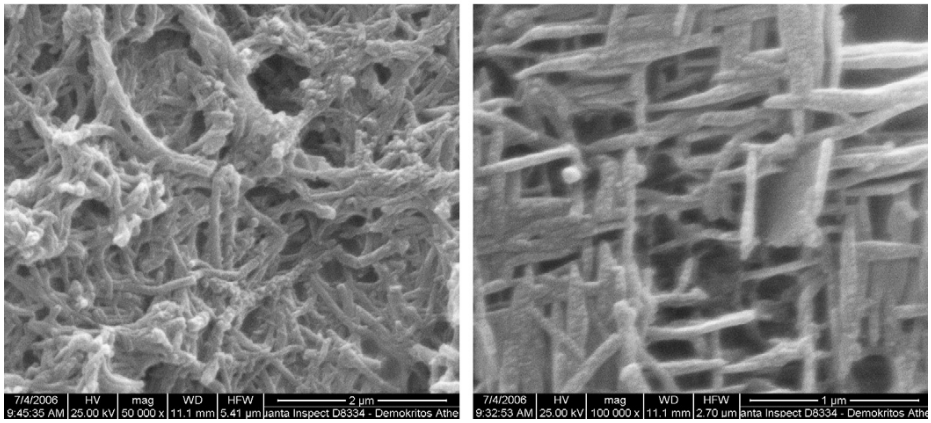

Figure 3.

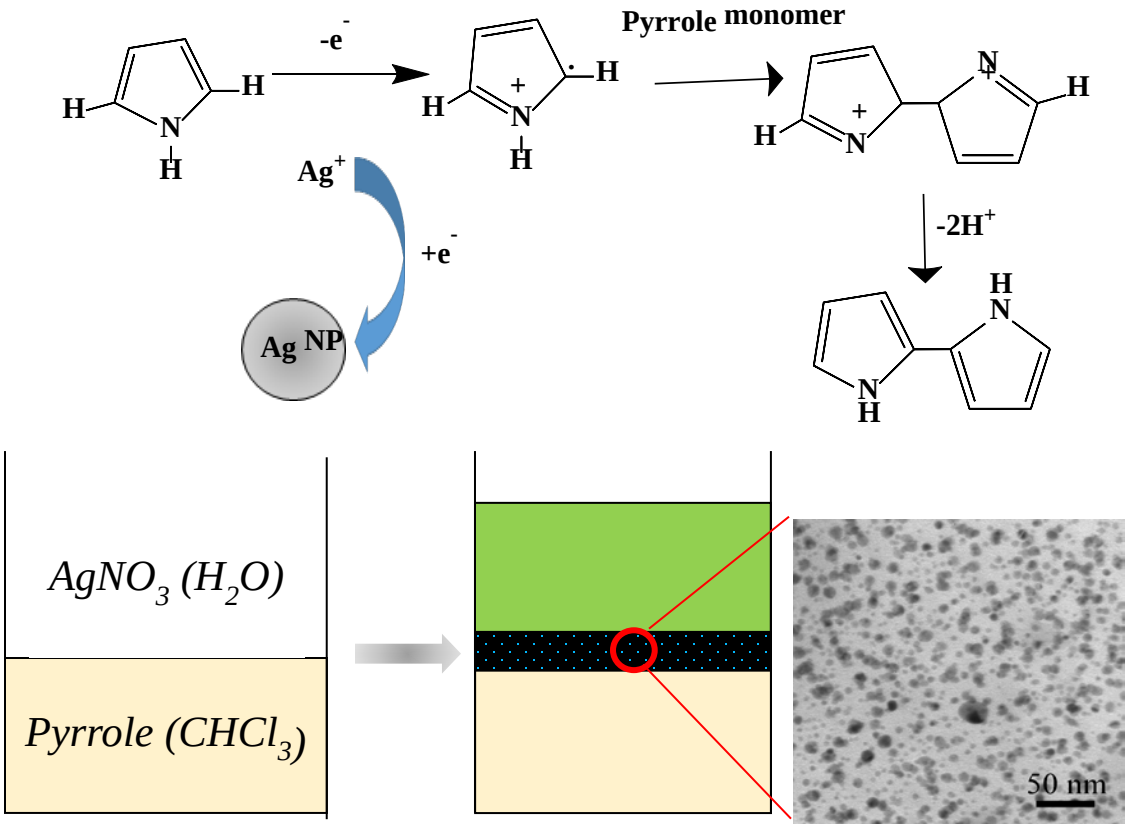

Figure 4.

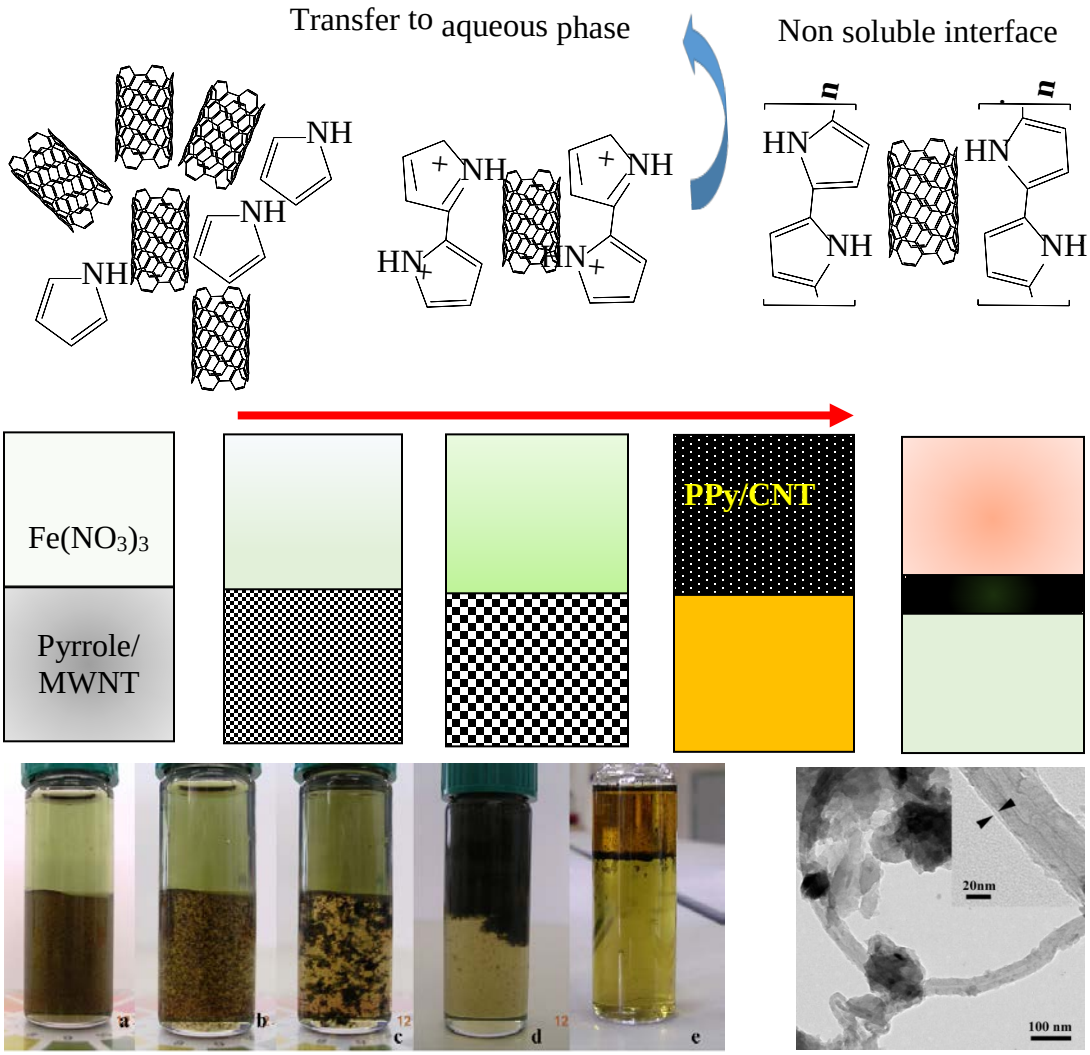
Transfer to aqueous phase
Non soluble interface
NH
NH
NH
HN
NH
NH
HN
NH
n
HN
NH
n
HN
NH
Fe(NO3)3
Pyrrole/
MWNT
PPy/CNT
a
b
c
d
e
20nm
100 nm

Figure 5.

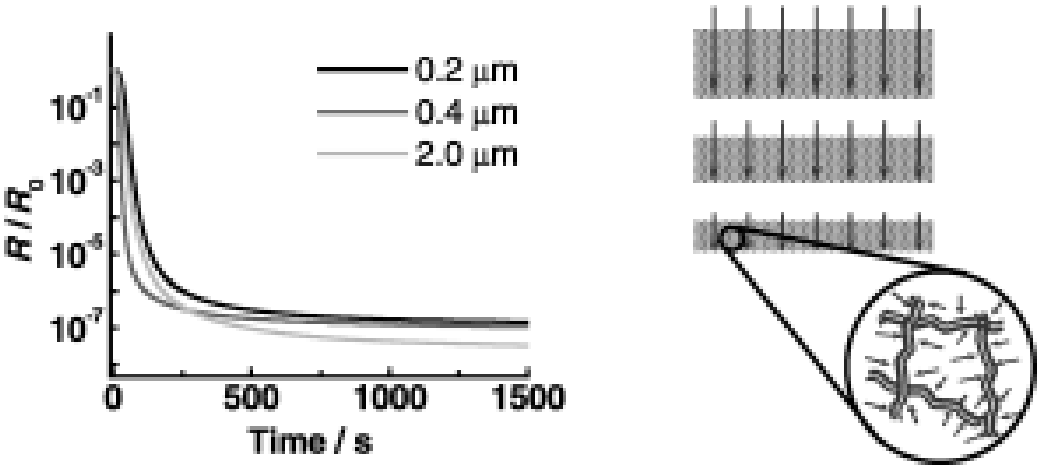

Figure 6.

Material	Conductivity
Noble metals (Cu, Au, Ag)	10^{5}-10^{6} S/cm
Polyacetylene	10-10^{4} S/cm
Polyaniline	10^{-1}-10^{3} S/cm
Polypyrrole	10^{-1}-10^{2} S/cm
Polystyrene	10^{-11}-10^{-10} S/cm
Nylon	10^{-12} S/cm

II.

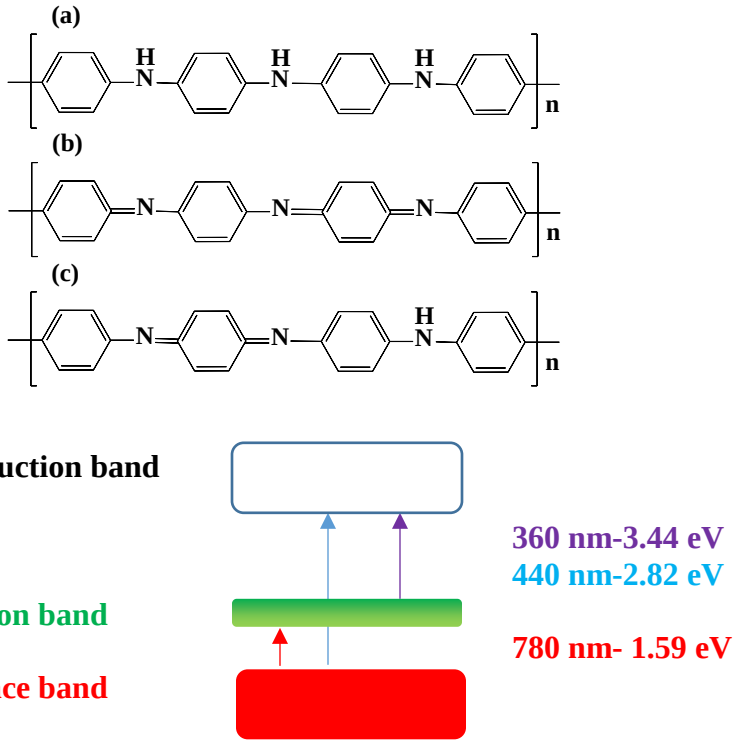

Figure 7.

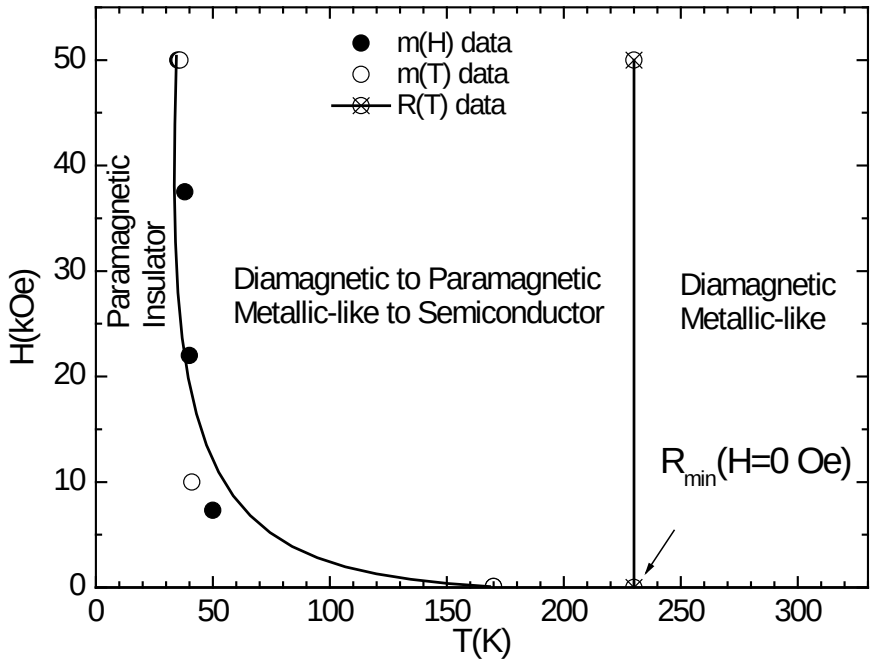
m(H) data
m(T) data
R(T) data
Paramagnetic
Insulator
Diamagnetic to Paramagnetic
Metallic-like to Semiconductor
Diamagnetic
Metallic-like
R_min(H=0 Oe)
H(kOe)
T(K)
0
10
20
30
40
50
0
50
100
150
200
250
300

Figure 8.

Hagen- Rubens model:

$R=1-2\sqrt{[(2\varepsilon_0 \cdot \omega)/\sigma]}$

Drude model:

$\sigma =(\omega^2\tau/4\pi)(1+ \omega^2 +\tau^2)^{-1}$

Drude model:

$\varepsilon(\omega)= \varepsilon_\infty - \omega^2\tau^2(1+ \omega^2 +\tau^2)^{-1}$

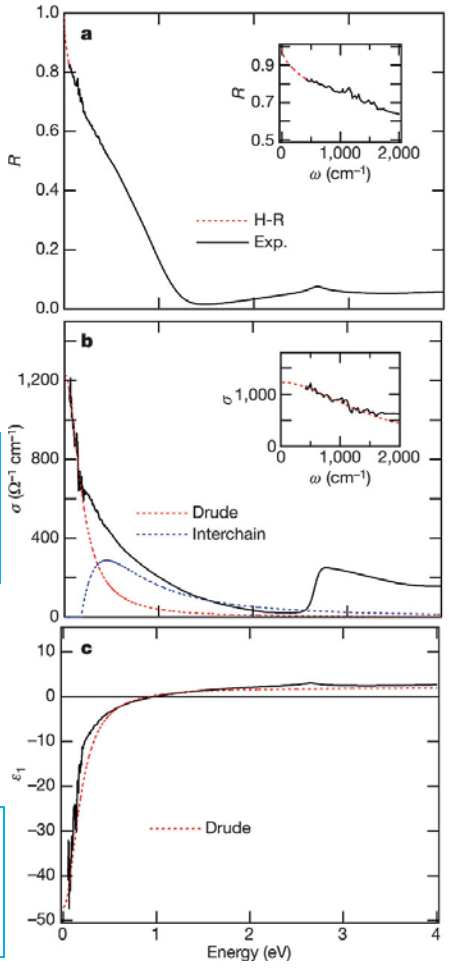

Figure 9.

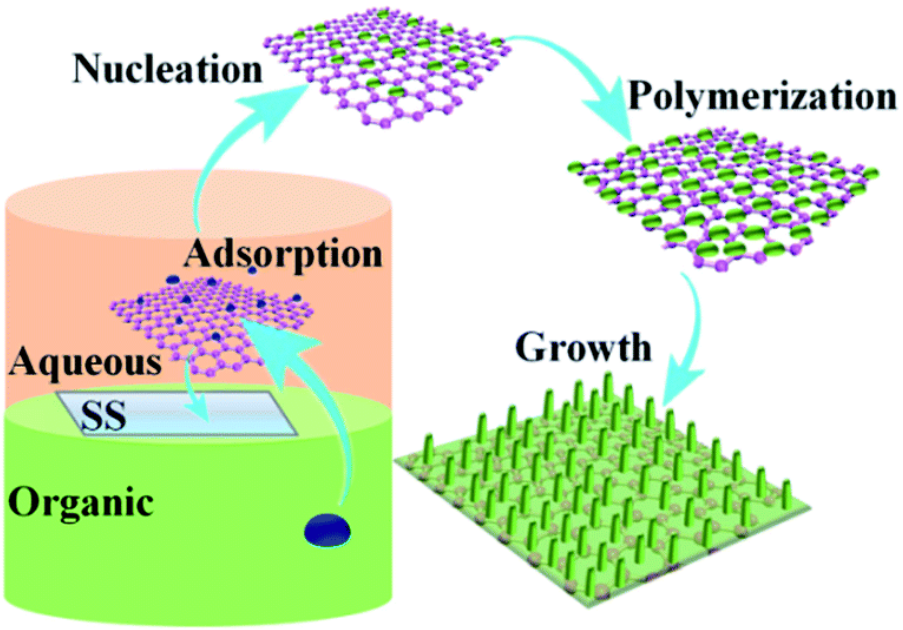
Nucleation
Polymerization
Adsorption
Aqueous
SS
Organic
Growth

Figure 10.